Electronic and magnetic properties of Gd-doped EuO

Masao Takahashi*
Kanagawa Institute of Technology, 1030 Shimo-Ogino, Atsugi-shi, 243-0292, Japan
(Received 30 March 2012; published 22 October 2012)

To study electron states and magnetism in Gd-doped EuO theoretically, we first calculate the spin-polarized density of states (DOS) by applying the dynamical coherent potential approximation (dynamical CPA) for two simple models: the s-f model of electron-doped EuO and a model of $Eu_{1-x}Gd_xO$. On the basis of the spin-polarized DOS, we calculate the total energy of electrons interacting with f spins through an exchange interaction. Then, we obtain the magnetization as a function of the temperature T, by minimizing the free energy. We discuss the mechanism of the electron-induced increase in the Curie temperature T_C, the origin of the anomalous magnetization curve, and the existence of a threshold Gd concentration for increasing T_C. We investigate the effect of on-site attractive potential that yields an impurity level when the Gd concentration is low. We also discuss the relationship between the redshift of the optical absorption edge and the increase in the T_C of Gd-doped EuO.

DOI: 10.1103/PhysRevB.86.165208 PACS number(s): 71.70.Gm, 75.25.−j, 75.50.Pp

I. INTRODUCTION

Europium oxide (EuO) is a typical Heisenberg-type ferromagnetic semiconductor with a rock-salt crystal structure.[1] It has been known since the 1960s that the Curie temperature T_C of EuO increases when EuO is doped with Gd.[2] Each Gd^{3+} ion substituted for the Eu^{2+} ion in EuO acts as a donor and donates one electron to the EuO conduction band. Conduction electrons mediate and enhance the exchange interaction between localized spins at the Eu site, resulting in an increase in T_C. Numerous studies have been carried out to characterize and optimize the doping-induced magnetic properties. Their results, however, vary appreciably. The reported maximum T_C of Gd-doped EuO ranges from 115 to 170 K.[3–12] The temperature dependence of magnetization also differs from one study to another. Many of these uncertainties are probably caused by problems with stoichiometry.

For spintronic applications, research interest in Gd-doped EuO has been renewed in recent years with modern techniques and improved sample quality. In particular, the success of preparing high-quality Gd-doped EuO samples over a wide range of doping levels has revealed some specific properties of Gd-doped EuO. The features of magnetic properties reported by Sutarto *et al.* are summarized as follows.[13] (a) With increasing Gd concentration x, T_C starts to increase and reaches a maximum of 125 K at $x \simeq 7\%$. With further Gd doping up to $x \simeq 20\%$, T_C decreases. (b) The temperature dependence of the magnetization of EuO follows the standard magnetization curve derived by applying the molecular field approximation (MFA) to the Heisenberg-type Hamiltonian using a Brillouin function. Upon Gd doping, the magnetization curve deviates strongly from the standard curve. For $x \simeq 7\%$, the magnetization curve again approaches the standard curve. Further doping with Gd up to $x \simeq 20\%$ results in a complete departure of the magnetization curve from the standard curve. (c) Only a low x is needed to directly increase T_C. T_C increases steadily as a function of x, reaching a maximum of 125 K. No threshold behavior is observed for x as low as 0.2%.

A maximum T_C for a certain dopant concentration x and magnetization showing an anomalous curve have been experimentally observed not only in Gd-doped EuO[13] but also in La-doped EuO,[14] Ce-doped EuO,[15] and Eu-rich EuO.[16] Therefore these phenomena are commonly observed in electron-doped EuO.

However, Mairoser *et al.* raised a question regarding the widespread assumption that every doped Gd ion donates one electron to the EuO conduction band.[17] They pointed out that only a small fraction of introduced Gd may donate electrons to the conduction band (i.e., $n < x$) and inferred that no maximum T_C as a function of n has been found, although T_C shows a maximum if plotted as a function of x. Furthermore, they showed that a minimum electron density n is required to increase T_C, i.e., $n \sim 1 \times 10^{19}$ cm^{-3}.

A theoretical study of the magnetic properties of Gd-doped EuO was performed by Mauger and coworkers.[6,8,18] By a treatment similar to the Ruderman-Kittel-Kasuya-Yosida (RKKY) theory but taking into account some specific features such as the spin-splitting of the band, Mauger and coworkers showed T_C as a function of the Gd concentration x. The theory of Mauger and coworkers, however, does not explicitly include the effect of magnetic impurity states. Regarding Gd impurities with Anderson impurities with a local level below the chemical potential, Arnold and Kroha studied the transport and magnetic properties of Gd-doped EuO.[19] The obtained results, however, are restricted within a dilute-doping region.

In addition, the energy of the optical absorption edge of a ferromagnetic (FM) semiconductor lowers with decreasing temperature; this phenomenon is known as the magnetic redshift. The total redshift of EuO is 0.27 eV.[1] Upon Gd doping, the total redshift of Gd-doped EuO decreases, although conflicting results have been reported for the dopant dependence of the absorption edge in the paramagnetic (PM) state.[5,10] The relationship between the increase in T_C and the behavior of the absorption edge of Gd-doped EuO has not yet been clarified.

In the present study, therefore, we intend to answer the following six questions consistently. (i) Is there an intrinsic limit to the electron-induced increase in T_C? If there is, what are the conditions for determining the electron density n_M that gives the maximum T_C? (ii) What causes anomalous magnetization? (iii) Is there a minimum n_c or x_c for inducing

a measurable increase in T_C? (iv) How does the attractive potential between the electron and the Gd donor center affect the magnetic properties of Gd-doped EuO? (v) How does it affect the magnetic properties of Gd-doped EuO when the electron density n is smaller than the Gd concentration x? (vi) How is the increase in T_C related to the redshift of the optical absorption edge in Gd-doped EuO?

In our previous work,[20] we studied the magnetic properties of electron-doped EuO by applying a virtual crystal approximation (VCA) to the s-f model. The result indicated the limitation of the VCA; the n dependence of T_C calculated by the VCA cannot explain the experimental observation. In the present study, therefore, we study electron-doped EuO by applying the dynamical coherent potential approximation (dynamical CPA) to the s-f model. For Gd-doped EuO, we propose a model Hamiltonian of $Eu_{1-x}Gd_xO$ that is an extension of the s-f model but includes the term of the nonmagnetic on-site potential introduced by randomly replacing the Eu^{2+} ion with the Gd^{3+} ion in EuO. In order to study the electronic and magnetic properties, we first calculate the spin-polarized density of states (DOS) by applying the dynamical CPA to the simple models above. Assuming that the electrons are degenerate, we next calculate the total energy of the electrons interacting with localized spins through an exchange interaction to obtain the free energy as a function of the normalized magnetization ($\langle S_z\rangle/S$). Then, we obtain the magnetization as a function of the temperature T under the condition in which the free energy is a minimum.

This paper is organized as follows. In Sec. II, we first explain the s-f model for electron-doped EuO and propose a model Hamiltonian for $Eu_{1-x}Gd_xO$. Then, we briefly formulate the dynamical CPA in the locator formula and explain the calculation of the magnetization and T_C. We present the results separately for the two models. In Sec. III, we give the results and discuss the electronic and magnetic properties of electron-doped EuO. In Sec. IV, we present the results for $Eu_{1-x}Gd_xO$ to study the effects of the on-site potential on the Gd site. We first investigate the magnetic impurity state and/or the magnetic tail that occurs in the dilute dopant region in detail (see Sec. IV A). Next, we investigate the electronic and magnetic properties over a wide range of Gd doping levels (see Sec. IV B). We devote Sec. IV C to the relationship between the optical absorption edge and the increase in the T_C of Gd-doped EuO. We present concluding remarks in Sec. V.

II. BASIC CONSIDERATION

A. Model Hamiltonian for electron-doped EuO

In pure EuO, localized magnetic spins (hereafter referred to as f spins) are set at regular lattice sites, and the exchange interaction between f spins is well described by the Heisenberg-type Hamiltonian

$$H_f = -\sum_{m,n} J_{mn}\mathbf{S}_m\cdot\mathbf{S}_n\ . \tag{1}$$

The notations here are conventional and the same as those in previous papers.[21,22] The application of the MFA to Eq. (1) gives the Curie temperature of EuO as

$$T_0 = \frac{2zJS(S+1)}{3k_B}\ . \tag{2}$$

When an electron is injected into EuO, the electron enters a broad conduction band.[23] The conduction band consists of $5d6s$ orbitals of the Eu^{2+} ion and the bottom of the conduction band exists at X points of triple degeneration.[24,25] In the simplified model, by disregarding the triplication and anisotropy of the band, a single band is usually assumed for the conduction band. Thus the conduction electron is referred to as the $s$electron in the model. An $s$electron moves in the crystal while interacting with localized f spins through an s-f exchange interaction. The s-electron state in EuO is well described by the s-f model Hamiltonian

$$H_{sf} = \sum_{m,n,\mu}\varepsilon_{mn}a^\dagger_{m\mu}a_{n\mu} - I\sum_{n,\mu,\nu}a^\dagger_{n\mu}\boldsymbol{\sigma}_{\mu\nu}\cdot\mathbf{S}_n a_{n\nu} + H_f. \tag{3}$$

The first term of Eq. (3) represents the kinetic energy of an s electron. In the second term, the s-f exchange interaction between an s electron and localized spin $\mathbf{S}_n$ of Eu site n is expressed in the simplest intra-atomic form; I is the exchange constant and $\boldsymbol{\sigma}_{\mu\nu}$ is the matrix component of the Pauli matrix of the s-electron spin. The model described by Eq. (3) is sometimes referred to as the Kondo lattice model.[26–32]

B. Model Hamiltonian for $Eu_{1-x}Gd_xO$

We regard Gd-doped EuO as $Eu_{1-x}Gd_xO$; the mole fraction x of Eu^{2+} ions in EuO is replaced at random with Gd^{3+} ions. The Gd^{3+} ion has the same electronic configuration as the Eu^{2+} ion and thus has the localized f spin of $S = 7/2$,[12] but donates one electron and acts as a donor center in EuO. In the present model, we assume that both J_{mn} and ε_{mn} are unchanged even if Eu^{2+} is replaced by Gd^{3+} at the mth and/or nth site in EuO. Furthermore, we assume that, at the Gd site, the s electron is subject to a local potential that involves not only an s-f exchange interaction but also a Coulomb interaction. Therefore, extending the s-f model for EuO, we study the s-electron states in Gd-doped EuO using the total Hamiltonian

$$H_t = H + H_f\ , \tag{4}$$

with

$$H = \sum_{m,n,\mu}\varepsilon_{mn}a^\dagger_{m\mu}a_{n\mu} + \sum_n u_n\ , \tag{5}$$

where u_n is either u_n^{Eu} (at the Eu site) or u_n^{Gd} (at the Gd site) depending on the ion species occupying the nth site:

$$u_n^{\mathrm{Eu}} = -I\sum_{\mu,\nu}a^\dagger_{n\mu}\boldsymbol{\sigma}_{\mu\nu}\cdot\mathbf{S}_n a_{n\nu}\ , \tag{6}$$

$$u_n^{\mathrm{Gd}} = -E_C\sum_{\mu}a^\dagger_{n\mu}a_{n\mu} - I\sum_{\mu,\nu}a^\dagger_{n\mu}\boldsymbol{\sigma}_{\mu\nu}\cdot\mathbf{S}_n a_{n\nu}\ . \tag{7}$$

Note that we assume the same exchange constant I for both Gd and Eu sites. In brief, the difference between u_n^{Eu} and u_n^{Gd} is the absence/presence of on-site potential E_C. When $x = 0$ and/or $E_C = 0$, the Hamiltonian H_t accords with H_{sf}.

C. Dynamical coherent potential approach (CPA)

Here, we briefly outline the dynamical CPA using the renormalized interactor formalism that we have employed in the present study.[21,33] We consider H instead of H_t to study the s-electron states, because the magnetic excitation energy is very small compared with the conduction bandwidth and s-f exchange energy. Thus we treat the single-particle Green's function defined by

$$G(\omega) = \frac{1}{\omega - H} . \tag{8}$$

Hereafter, the variable ω will sometimes be omitted from the operators [$G \equiv G(\omega)$].

The site-diagonal component of G in the Wannier representation $\langle n\mu|G(\omega)|n\mu\rangle$ describes the hopping of an s electron with a μ spin starting and ending at the nth site. Thus $\langle n\mu|G(\omega)|n\mu\rangle$ depends not only on the species of occupant at the nth site but also on the configuration surrounding the nth site. An s electron moving in Gd-doped EuO is subjected to disordered potentials that arise not only from substitutional disorder but also from thermal fluctuations of f spins through the s-f exchange interaction. Furthermore, when magnetization arises, the effective potential for the s-electron differs according to the orientation of the s-electron spin. In the dynamical CPA using locator formalism, the disordered potential is taken into account in terms of the spin-dependent effective medium described by the coherent potential Σ_μ and the site-renormalized interactor J_μ, where J_μ represents the transfer of an s electron with a spin μ between the n-th site and the surrounding effective medium Σ_μ. J_μ depends on Σ_μ but not on the occupation of the nth site itself. It can be shown that the quantity J_μ is expressed as the change in the energy of an s electron at the nth site owing to its interaction with the surrounding effective medium.[34,35]

The spin-flip/spin-nonflip process of an s electron through the s-f exchange interaction with the f spin at the nth site is taken into consideration in the single-site approximation. Hereafter, we express the site-diagonal elements of G as $\langle n|G^{\mathrm{Gd}}|n\rangle$ when the real potential of u_n^{Gd} is embedded at site n in the effective medium. Then, G^{Gd} is expressed by

$$G^{\mathrm{Gd}} = \frac{1}{\omega - u_n^{\mathrm{Gd}} - \sum_\mu J_\mu a_{n\mu}^\dagger a_{n\mu}} . \tag{9}$$

Note that G^{Gd} is a 2×2 matrix in spin indices, whose matrix element $\langle\mu|G^{\mathrm{Gd}}|\nu\rangle$ is written as $G_{\mu\nu}^{\mathrm{Gd}}$ hereafter. The explicit expression for $G_{\mu\nu}^{\mathrm{Gd}}$ is given in Eq. (A3) of Appendix A. Note that the spin-diagonal element of $G^{\mathrm{Gd}}(S_z)$ takes the value of $G_{\mu\mu}^{\mathrm{Gd}}(S_z)$, where S_z is the eigenvalue of the z-component of the f spin; $S_z = -S, \ldots, +S$. Thus the thermal average of $G_{\mu\mu}^{\mathrm{Gd}}$ over a fluctuating f spin, $F_\mu^{\mathrm{Gd}}(\omega)$, is calculated by the MFA using

$$F_\mu^{\mathrm{Gd}}(\omega) \equiv \left\langle G_{\mu\mu}^{\mathrm{Gd}} \right\rangle = \sum_{S_z=-S}^{S} G_{\mu\mu}^{\mathrm{Gd}}(S_z) \exp(\lambda S_z) \Big/ \sum_{S_z=-S}^{S} \exp(\lambda S_z) , \tag{10}$$

where λ is determined so as to reproduce the given $\langle S_z\rangle$ as

$$\langle S_z\rangle = \sum_{S_z=-S}^{S} S_z \exp(\lambda S_z) \Big/ \sum_{S_z=-S}^{S} \exp(\lambda S_z). \tag{11}$$

Note that we assume the same $\lambda(\equiv h/k_B T)$ for both Eu and Gd sites in this study, where h is the effective field to which the localized f spins are subjected; T is the temperature. Since there is a one-to-one correspondence between $\langle S_z\rangle$ and the parameter λ, we can describe the s-electron states in terms of $\langle S_z\rangle$ instead of λ.

Here, we suppose that the coherent potential Σ_μ is set at the n-th site in the effective medium. Then, the diagonal component of the reference propagator in the Wannier representation is simply obtained as (independent of n)

$$F_\mu(\omega) = \frac{1}{\omega - \Sigma_\mu - J_\mu} . \tag{12}$$

The situation supposed here is equivalent to that an s-electron is moving in the effective medium Σ_μ. Thus $F_\mu(\omega)$ is equal to the diagonal component of $P \equiv 1/(1-K)$ in the Wannier representation, where K is the reference Hamiltonian for describing an s electron moving in the effective medium Σ_μ. Therefore $F_\mu(\omega)$ is calculated as

$$F_\mu(\omega) = \langle n\mu|P(\omega)|n\mu\rangle = \int_{-\Delta}^{\Delta} \frac{D_0(\varepsilon)}{\omega - \varepsilon - \Sigma_\mu} d\varepsilon , \tag{13}$$

where $D_0(\omega)$ is an undisturbed DOS. Throughout this work, we assume the model DOS of semicircular form with a half bandwidth Δ,

$$D_0(\varepsilon) = \frac{2}{\pi\Delta}\sqrt{1 - \left(\frac{\varepsilon}{\Delta}\right)^2} , \tag{14}$$

as an undisturbed DOS. By using Eqs. (12)–(14), we obtain the following simple relation between J_μ and F_μ:

$$J_\mu = \frac{\Delta^2}{4} F_\mu . \tag{15}$$

In accordance with the CPA, we determine J_μ self-consistently. The dynamical CPA condition using the renormalized interactor formalism is finally given by

$$F_\uparrow(\omega) = (1-x)F_\uparrow^{\mathrm{Eu}}(\omega) + x F_\uparrow^{\mathrm{Gd}}(\omega) , \tag{16a}$$

$$F_\downarrow(\omega) = (1-x)F_\downarrow^{\mathrm{Eu}}(\omega) + x F_\downarrow^{\mathrm{Gd}}(\omega) . \tag{16b}$$

The procedure for the numerical calculation is as follows. When F_μ is given, J_μ is simply calculated using Eq. (15). Then, F_μ^{Gd} is calculated using Eq. (10); F_μ^{Eu} is also calculated in a similar way. Consequently F_μ is again obtained using Eq. (16). Therefore F_μ and J_μ are determined self-consistently. This procedure is repeated until the calculation converges. It is also worth noting that, in the calculations of F_μ^{Gd}, both $J_\uparrow$ and $J_\downarrow$ are used as a consequence that the spin flip processes are properly taken into account. Therefore we need to solve Eqs. (16a) and (16b) simultaneously. No other special methods/techniques are needed to numerically solve the dynamical CPA equations above. We have also calculated the t value of $|t| \equiv |xt^{\mathrm{Gd}} + (1-x)t^{\mathrm{Eu}}|$ (see Ref. 21) and verified that the value is as small

as $|t| \lesssim 10^{-10}\Delta$. The DOS with a μ spin, $D_\mu(\omega)$, is calculated using

$$D_\mu(\omega) = -\frac{1}{\pi}\mathrm{Im}F_\mu(\omega)\,. \tag{17}$$

The advantage of the CPA using the renormalized interactor formalism is that it is straightforward to determine the species-resolved DOS, i.e., the local DOS associated with each type of ion in the alloy. The local DOS with a μ spin at the Gd site is denoted as $D_\mu^{\mathrm{Gd}}(\omega)$; $xD_\mu^{\mathrm{Gd}}(\omega)$ is referred to as the Gd-component DOS.

Furthermore, to gain insight into the origin and mechanism of the increase in T_C, we also calculate the spin-coupling strength $Q(\omega)$ at the Gd (Eu) site defined by

$$Q(\omega) = \left.\frac{\langle\delta(\omega - H)\boldsymbol{\sigma}\cdot\boldsymbol{S}\rangle/S}{\langle\delta(\omega - H)\rangle}\right|_{\mathrm{Gd(Eu)-site}}. \tag{18}$$

The explicit expression for $Q(\omega)$ is given in Appendix B. Roughly speaking, $Q(\omega)$ corresponds to $\langle\cos\theta\rangle$, where θ is the angle between the spin of an s electron with energy ω and the localized f spin. When $Q(\omega) \approx 1$, the s-electron spin is strongly coupled parallel to the f spin, so that the maximum energy gain due to the s-f exchange interaction is obtained. The energy gain induces magnetization and increases T_C. In contrast, $Q(\omega) \approx -1$ means that the s-electron spin is coupled antiparallel to the f spin, and $Q(\omega) \approx 0$ means that the s-electron spin is independent of the direction of the f spin. Therefore $Q(\omega)$ represents the manner and/or degree of coupling between the s-electron spin and the f spin, and the result for $Q(\omega)$ can give a clue to investigating the relationship between the magnetism and s-electron states in electron-doped EuO and/or Gd-doped EuO.

D. Magnetization and Curie temperature

Here, we show the present procedure for calculating the normalized magnetization $\langle S_z\rangle/S$ as a function of the temperature T for various s-electron densities n. Throughout this paper, we assume that s electrons are degenerate. Then, we obtain the s-electron density n per site and the total energy $E(\langle S_z\rangle)$ as

$$n = \int_{-\infty}^{\varepsilon_{\mathrm{F}}} [D_\uparrow(\omega) + D_\downarrow(\omega)]d\omega\,, \tag{19}$$

$$E(\langle S_z\rangle) = \int_{-\infty}^{\varepsilon_{\mathrm{F}}} \omega[D_\uparrow(\omega) + D_\downarrow(\omega)]d\omega\,, \tag{20}$$

respectively, as functions of the energy of the Fermi level ε_{F}. Note that the dependence of $E(\langle S_z\rangle)$ on $\langle S_z\rangle$ is contained in $D_\mu(\omega)$, and that $E(\langle S_z\rangle)$ is the sum of the kinetic and exchange energies. For a fixed $\langle S_z\rangle/S$, the total s-electron density n ($\equiv n_\uparrow + n_\downarrow$) has a one-to-one correspondence with ε_{F}, and therefore $E(\langle S_z\rangle)$ can be obtained as a function of n. Therefore the free energy per site of the system is given as

$$F(\langle S_z\rangle) = E(\langle S_z\rangle) - zJ\langle S_z\rangle^2 - T\mathcal{S}, \tag{21}$$

where the entropy due to localized f spins is given by

$$\mathcal{S} = k_B \log \sum_{S_z=-S}^{S} \exp\left(\frac{h}{k_B}S_z\right) - \frac{h}{T}\langle S_z\rangle\,. \tag{22}$$

The effective field h is determined so as to minimize $F(\langle S_z\rangle)$ through the condition

$$\frac{d}{dh}F(\langle S_z\rangle) = 0\,. \tag{23}$$

First, from condition (23), we obtain h as a function of $\langle S_z\rangle$; $h \equiv h_1 + h_2$, where h_1 is the molecular field induced by the surrounding f spins and given by

$$h_1 = 2zJ\langle S_z\rangle = \frac{3k_BT_0}{S(S+1)}\langle S_z\rangle, \tag{24}$$

and h_2 is the effective field due to spin-polarized electron density via an s-f exchange interaction and given by

$$h_2 = -\frac{d}{d\langle S_z\rangle}E(\langle S_z\rangle)\,. \tag{25}$$

Next, we obtain the normalized magnetization $\langle S_z\rangle/S$ as a function of T by varying $\langle S_z\rangle$ so as to give the minimum $F(\langle S_z\rangle)$. In actual calculations, we calculated the values of $E(\langle S_z\rangle)$ for $\langle S_z\rangle/S = 0.00, 0.01, \ldots, 1.00$ and interpolated them to obtain h_2 as a function of $\langle S_z\rangle$. We have verified that $\langle S_z\rangle = SB_S(hS/k_BT)$ is satisfied, where $B_S(x)$ is the Brillouin function.

E. Parameters for EuO and $Gd_xEu_{1-x}O$

In this study, we put $S = 7/2$ for localized f spins and $T_0 = 70$ K for the Curie temperature of pure EuO.[1] We take the exchange energy $IS = I_{df} \times S = 0.1 \times 7/2 = 0.35$ eV, which was estimated from the difference between the atomic energy levels for a $5d$ electron parallel and antiparallel to the $4f^7$ state.[1] For the conduction band, we assume a broad bandwidth of $2\Delta = 7.0$ eV (i.e., $IS/\Delta = 0.1$) so as to yield a magnetic redshift of 0.27 eV (see the discussion in Sec. IV C). Furthermore, we set the on-site potential $E_C = 0.5\Delta$ for a Gd ion so that, at PM temperatures, a shallow donor level appears below the bottom of the conduction band of EuO (see the discussion in Sec. IV A).

III. RESULTS AND DISCUSSION FOR ELECTRON-DOPED EUO

In Figs. 1–6, we show the present results for electron-doped EuO, which are calculated on the basis of the DOS obtained by applying the dynamical CPA to the s-f model Hamiltonian [see Eq. (3)]. In Fig. 1(a), the spin-polarized DOS of EuO is presented for $\langle S_z\rangle/S = 0.0, 0.2, 0.4, 0.6, 0.8$, and 1.0. Note that the present result for the DOS is different from the previous result obtained by the VCA (i.e., Fig. 2 in Ref. 20). In the VCA, the spin-polarized DOS is simply given by $D_\mu^{\mathrm{VCA}}(\omega) = D_0(\omega \pm I\langle S_z\rangle)$. In the PM state ($\langle S_z\rangle = 0.0$), therefore, the DOS obtained by the VCA agrees with the unperturbed model band $D_0(\omega)$, and the energy of the bottom of the band is given by $\omega_0 = -\Delta$. On the other hand, even in the PM state, the DOS shown in Fig. 1(a) broadens owing to f spin fluctuation through the exchange interaction.[22] As a consequence, the energy of the bottom of the band in the PM state is not $\omega_0 = -\Delta$ but $\omega_b = -1.0231\Delta$.[36] The difference between the DOSs obtained by the VCA and dynamical CPA may seem small, but it results in a significant difference in the n dependence of T_C, as shown below. With an increase in $\langle S_z\rangle/S$, the bottom of the

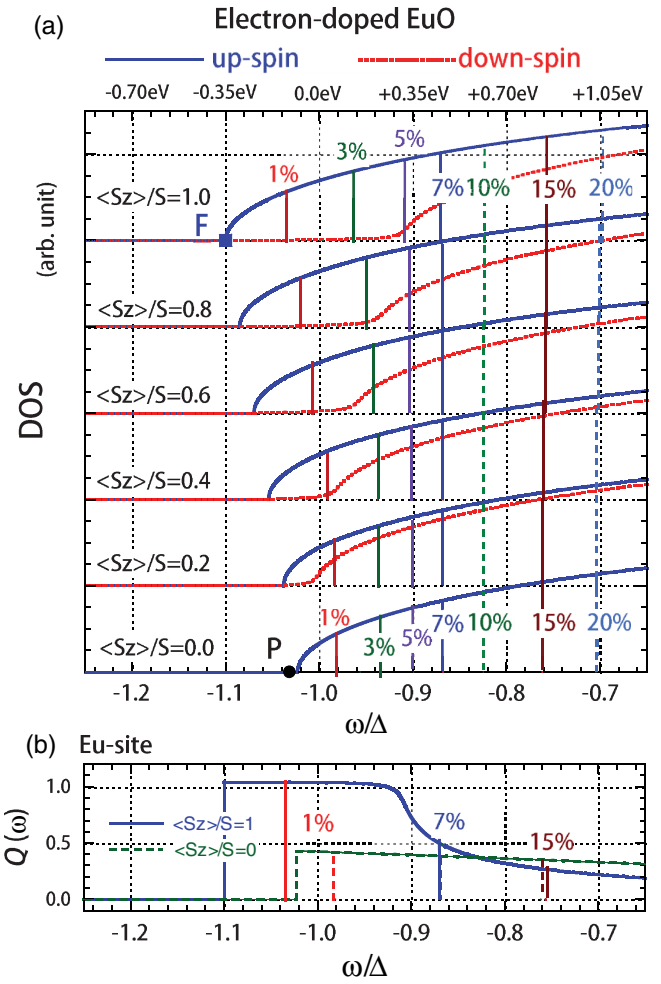

FIG. 1. (Color online) Results for electron-doped EuO. (a) Lower-energy part of the density of states (DOS) shown for magnetizations $\langle S_z\rangle/S = 0.0, 0.2, 0.4, 0.6, 0.8$, and 1.0. The solid line is for the up-spin band $D_\uparrow(\omega)$, and the dotted line is for the down-spin band $D_\downarrow(\omega)$. Along the upper abscissa, the values of $\omega + \Delta$ with $\Delta = 3.5$ eV are shown in electron Volts; note that the energy of the bottom of the model band ($\omega_0 = -\Delta$) is assigned to 0 eV. The vertical lines indicate the Fermi level ε_F for electron densities $n =$ 1.0, 3.0, 5.0, 7.0, 10, 15, and 20%. Dots P and F indicate the impurity levels when a Gd ion is used for doping at the paramagnetic and ferromagnetic temperatures, respectively (see text). (b) Spin-coupling strength $Q(\omega)$ at the Eu site shown for $\langle S_z\rangle/S = 0.0$ (dashed line) and $\langle S_z\rangle/S = 1.0$ (solid line). The Fermi levels ε_F for $n = 1.0, 7.0$, and 15% are indicated by vertical lines; the dotted line is for $\langle S_z\rangle/S = 0.0$ and the solid line is $\langle S_z\rangle/S = 1.0$.

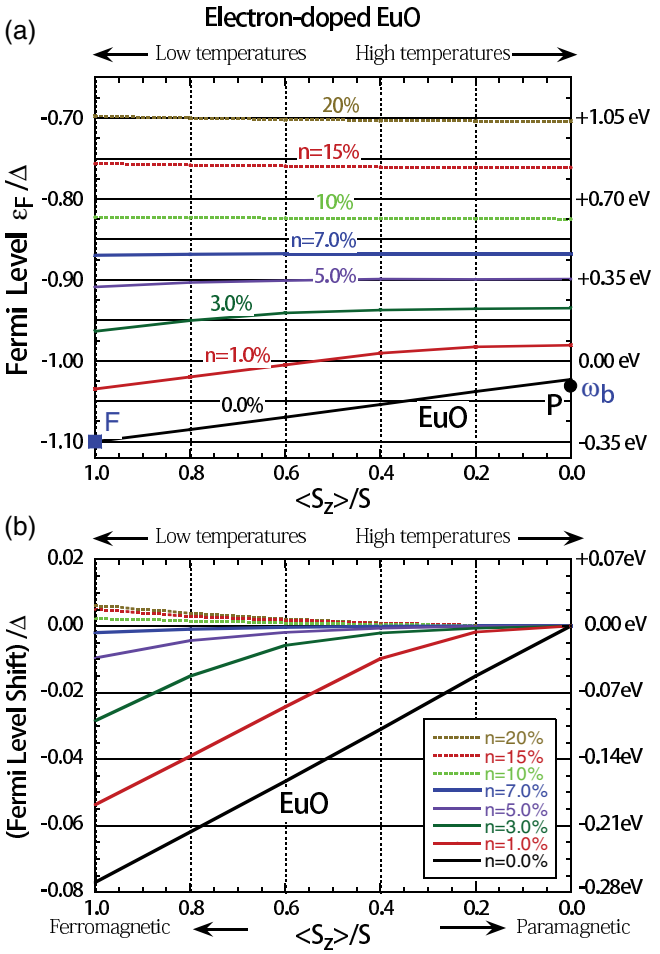

FIG. 2. (Color online) Results for electron-doped EuO with electron densities $n = 0.0, 1.0, 3.0, 5.0, 7.0, 10, 15$, and 20%. (a) Fermi level ε_F shown as a function of $\langle S_z\rangle/S$. Along the left ordinate, the scale for ε_F/Δ is shown, while along the right ordinate, the scale for the energy $\varepsilon_F + \Delta$ with $\Delta = 3.5$ eV is shown in electron volts; the bottom of the model band ($\omega_0 = -\Delta$) is assigned to 0 eV. (b) Energy shift of the Fermi level shown as a function of $\langle S_z\rangle/S$. Along the left ordinate, the scale for $[\varepsilon_F(\langle S_z\rangle/S) - \varepsilon_F(0)]/\Delta$ is shown, while along the right ordinate, the scale for the energy $\varepsilon_F(\langle S_z\rangle/S) - \varepsilon_F(0)$ with $\Delta = 3.5$ eV is presented in electron volts.

up-spin band stretches to the low-energy side, whereas the tail of the down-spin band shrinks to the high-energy side. In the completely FM state ($\langle S_z\rangle/S = 1$), the up-spin DOS agrees with $D_0(\omega + IS)$, whereas the down-spin DOS does not agree with $D_0(\omega - IS)$; the down-spin band has a tail down to the bottom of the band (i.e., $-\Delta - IS$), because the s electron with down spin can flip their spin under the condition that the total spin ($=S - 1/2$) is conserved if the DOS with the up spin is not zero therein.[22]

When electrons are doped into EuO, they preferentially enter the lower-energy part of the band and occupy the states from the bottom up to the Fermi level; the energy of the Fermi level ε_F is related to the electron density n by Eq. (19). In Fig. 1(a), we indicate the Fermi levels ε_F by the vertical lines. Note that the dependence of ε_F on $\langle S_z\rangle/S$ varies with n. To show this difference clearly, in Fig. 2(a), we present ε_F as a function of $\langle S_z\rangle/S$; $\varepsilon_F = \varepsilon_F(\langle S_z\rangle/S)$. To display the ε_F behavior more clearly, in Fig. 2(b), we show the energy shifts, which are defined as $\varepsilon_F(\langle S_z\rangle/S) - \varepsilon_F(0)$. From the figure, we find that with an increase in $\langle S_z\rangle/S$, ε_F with $n \lesssim 5\%$ shifts to the low-energy side, whereas ε_F with $n \gtrsim 10\%$ slightly shifts to the high-energy side. Since the total energy $E(\langle S_z\rangle)$ is defined by Eq. (20), the lowering of ε_F is closely related to the decrease in $E(\langle S_z\rangle)$. The decrease in $E(\langle S_z\rangle)$ with increasing $\langle S_z\rangle/S$ induces ferromagnetism and results in an increase in T_C.

To gain insight into the mechanism of magnetism in electron-doped EuO, in Fig. 1(b) we show the result for the spin-coupling strength $Q(\omega)$ defined by Eq. (18). Note that

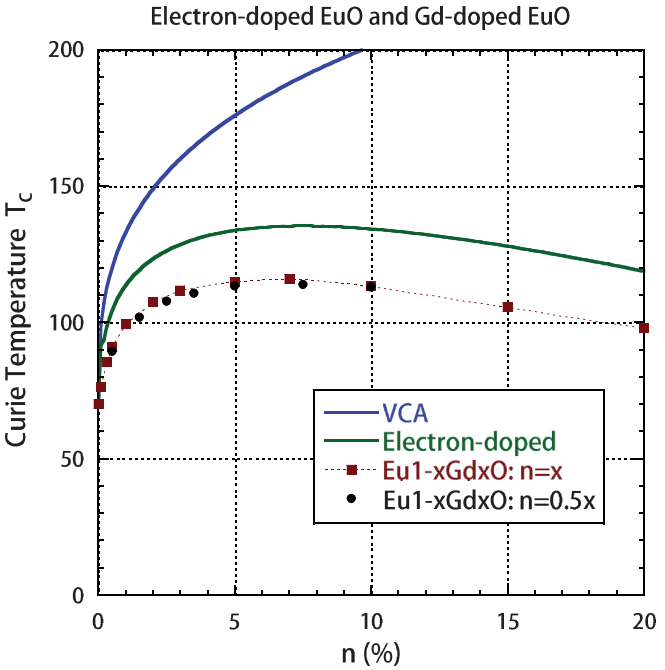

FIG. 3. (Color online) Curie temperature T_C calculated by applying the dynamical CPA for electron-doped EuO shown as a function of the electron density n, together with T_C obtained by the VCA or Eq. (26). Black squares ■ and black dots • represent the values of T_C calculated by applying the dynamical CPA for $Eu_{1-x}Gd_xO$ assuming $n = x$ and $0.5x$, respectively (see text).

$Q(\omega) \neq 0$ even when $\langle S_z \rangle = 0$, because in the dynamical CPA it is considered that the motion of the s-electron spin follows the motion of f spins to a certain degree. When $\langle S_z \rangle = 0$, $Q(\omega)$ has a finite positive value at energies ω near the bottom of the band, and $Q(\omega)$ gradually decreases with an increase in ω. In the FM state ($\langle S_z \rangle = S$), in contrast, $Q(\omega) \approx 1.0$ in the energy range of $-1.1 \leqq \omega/\Delta \lesssim -0.9$ (i.e., $-IS - \Delta \leqq \omega \lesssim +IS - \Delta$), and $Q(\omega)$ quickly decreases with increasing $\omega(\gtrsim -0.9\Delta)$. $Q(\omega) \approx 1.0$ means that the electron spin and f spin are almost parallel and that the gain of exchange energy is fully obtained. Note that the energy of $\omega = +IS - \Delta (= -0.9\Delta)$ is close to ε_F for $n = 5\%$. Therefore, when n is as small as $n \lesssim 5\%$, ε_F decreases with increasing $\langle S_z \rangle / S$, suggesting that T_C increases as n increases. In contrast, when $n \gtrsim 10\%$, $Q(\omega)$ for $\langle S_z \rangle / S = 1$ is somewhat smaller than that for $\langle S_z \rangle / S = 0$. Therefore, when $n \gtrsim 10\%$, ε_F slightly shifts to the high-energy side with an increase in $\langle S_z \rangle / S$, suggesting that the increase in n is accompanied by a slight decrease in T_C.

In Fig. 3, we present the result for the T_C of electron-doped EuO as a function of n. T_C, starting from $T_0 = 70$ K, increases quickly with an increase in n up to 5 %; T_C has a peak $T_C \approx 135$K at $n \approx 7\%$, and then decreases gradually for $n \gtrsim 10\%$. Therefore the discussion above on $Q(\omega)$ well explains the n dependence of T_C.

In Fig. 3, for comparison, we include the previous result for the Curie temperature calculated by the VCA; T_C^{VCA} is given by[20]

$$T_C^{\mathrm{VCA}} = T_0 + \frac{2}{3k_B}\left(1 + \frac{1}{S}\right)(IS)^2 D_0(\varepsilon_F)\,. \qquad (26)$$

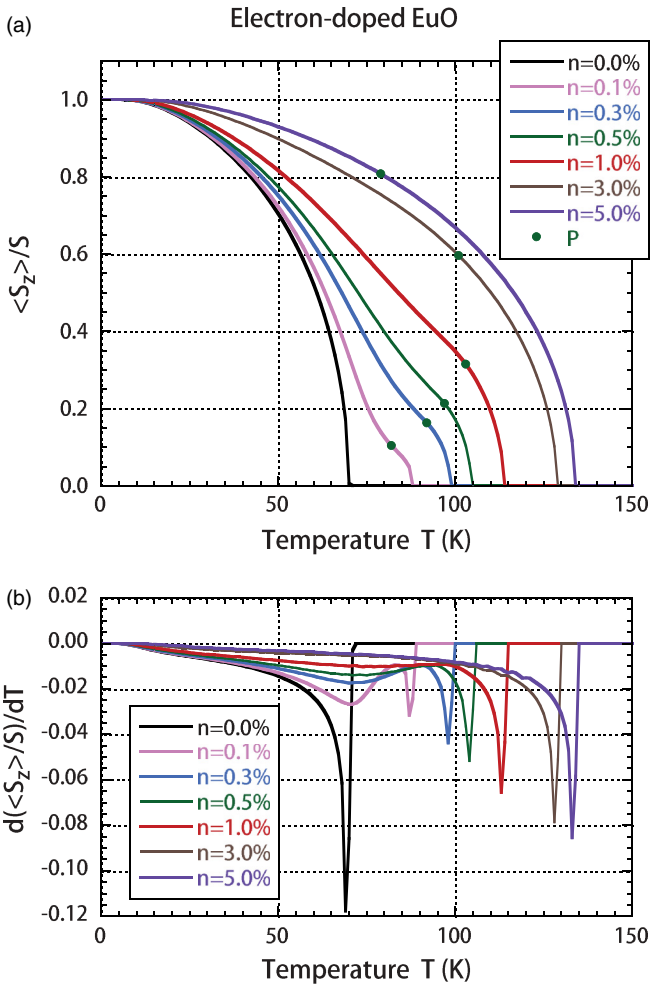

FIG. 4. (Color online) Results for electron-doped EuO with the electron densities $n = 0.0, 0.1, 0.3, 0.5, 1.0, 3.0$, and 5.0%. (a) Normalized magnetization $\langle S_z \rangle / S$ shown as a function of the temperature T. Points "P" represent "flexure points" indicating $n_\downarrow = 0.1 n_\uparrow$ (see text). (b) Temperature derivative of magnetization, $d(\langle S_z \rangle / S)/dT$, shown as a function of T.

Equation (26) shows that T_C^{VCA} increases monotonically with an increase in n. Therefore T_C^{VCA} cannot explain the n dependence of T_C experimentally observed. A significant difference of the VCA from the dynamical CPA is that, in the VCA, the correlated motion between the electron spin and the f spin is completely neglected [i.e., $Q(\omega)^{\mathrm{VCA}} = 0$] at PM temperatures; thus the energy gain due to the increase in $\langle S_z \rangle$ is overestimated.

In Figs. 4 and 5, we show the normalized magnetization curve $\langle S_z \rangle / S$ as a function of T. For $n = 0$ (or undoped EuO), the magnetization curve follows the standard curve with $T_C = T_0 \equiv 70$ K. With an increase in n, T_C increases from $T_0 = 70$ K, while the shape of the magnetization curve deviates strongly from the standard curve. In the magnetization curve with a low electron concentration of $n \lesssim 5\%$, two successive superimposed dome shapes appear with increasing temperature. For $n \gtrsim 5\%$, the magnetization curve again becomes closer to the standard curve (see Fig. 5). To show the features of the magnetization curve in more detail, we present the temperature derivative of the normalized magnetization

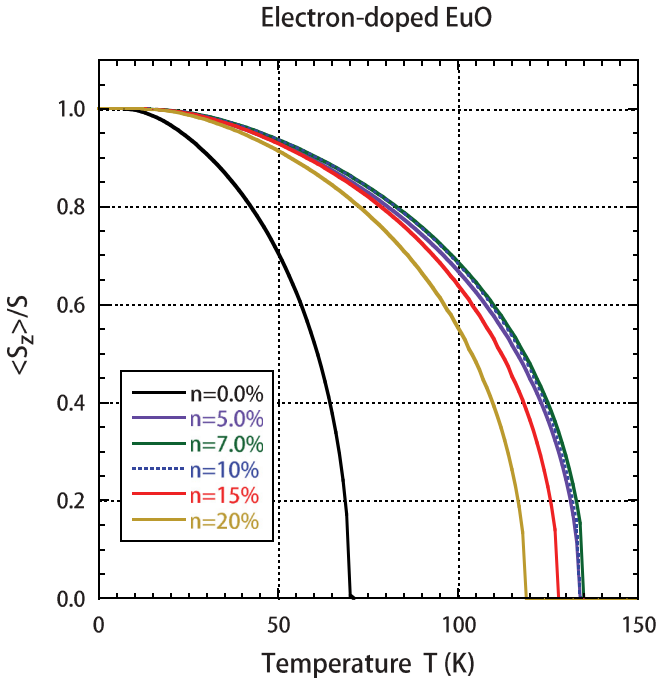

FIG. 5. (Color online) Result for electron-doped EuO. The normalized magnetization $\langle S_z\rangle/S$ with electron densities $n = 0.0, 5.0, 7.0, 10, 15$, and 20% is shown as a function of the temperature T.

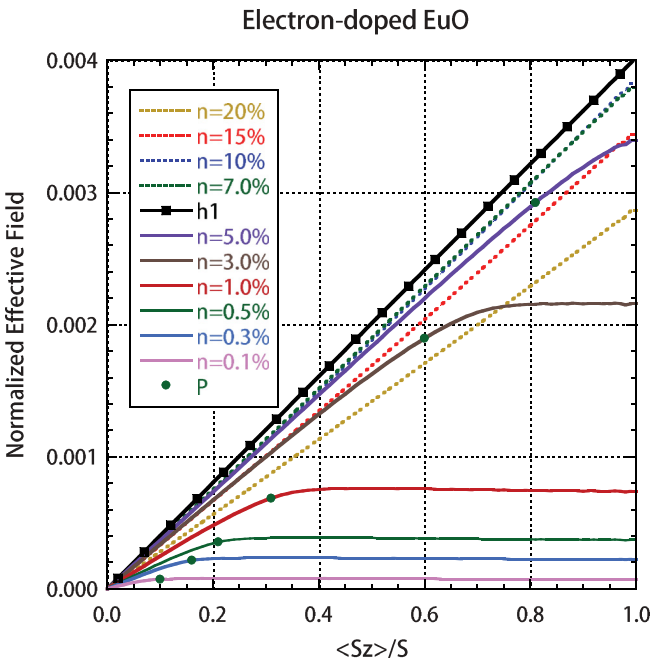

FIG. 6. (Color online) Result for electron-doped EuO. Normalized effective fields h_2S/Δ with various electron densities n and h_1S/Δ are shown as functions of $\langle S_z\rangle/S$; h_1 and h_2 are defined by Eqs. (24) and (25), respectively. Points "P" represent "flexure points" indicating $n_\downarrow = 0.1n_\uparrow$ (see text).

$d(\langle S_z\rangle/S)/dT$ in Fig. 4(b) as a function of the temperature T. One can clearly see sharp peaks at $T_0 = 70$ K for $n = 0.0\%$ and at the corresponding values of T_C for $n \gtrsim 5\%$. On the other hand, for $n \lesssim 5\%$, one can clearly distinguish two features: a peak at the corresponding values of T_C and a structure at a temperature slightly above T_0. Therefore the present result for the magnetization curve well reproduces the previously reported feature.[13–17]

To explain the origin of the anomalous magnetization, in Fig. 6, we show the effective fields h_1 and h_2 as functions of $\langle S_z\rangle/S$. When $n \gtrsim 5\%$, h_2 is proportional to $\langle S_z\rangle/S$; thus, the magnetization curve becomes the standard curve. In contrast, when $n \lesssim 5\%$, h_2 is initially proportional to $\langle S_z\rangle/S$ and then approaches a saturation value; the saturation value is somewhat smaller than In, although it is estimated as $h_2 = In$ in the VCA.[20] The relationship between n and the magnetization curve is roughly explained as follows. The spin-polarized band shifts proportionally to $\pm\langle S_z\rangle$ depending on its spin direction. When both up- and down-spin bands are populated, the transfer of electrons from the down-spin band to the up-spin band occurs accompanied by an increase in $\langle S_z\rangle$. The number of electrons transferred is proportional to $\langle S_z\rangle$. Consequently, the energy gain is proportional to $\langle S_z\rangle^2$, so that h_2 is proportional to $\langle S_z\rangle$, indicating that the magnetization follows the standard curve as in the case of $n \gtrsim 5\%$. In contrast, when $n \lesssim 5\%$, the situation differs depending on $\langle S_z\rangle$. If $\langle S_z\rangle$ is smaller than a certain value, both the up- and down-spin bands are populated, and then h_2 becomes proportional to $\langle S_z\rangle$. If $\langle S_z\rangle$ is larger than a certain value, however, no transfer of electrons from the down-spin band to the up-spin band occurs because few electrons occupy the down-spin states [see Fig. 1(a)]; thus the energy gain is proportional to $\langle S_z\rangle$, so that h_2 approaches its saturation value and acts as if it is an external field applied on the f spins. Therefore the magnetization curve is composed of two partial curves above and below a certain $\langle S_z\rangle$. In the VCA, the condition for the flexure points is given by $\langle S_z\rangle/S = n/2ISD_0(\varepsilon_F)$.[20] In the dynamical CPA, however, it is difficult to specify the condition, because the down-spin band has a tail that reaches the bottom of the up-spin band even at $T = 0$.[22] In Figs. 4(a) and 6, therefore, we plotted "flexure points P" under the condition that $n_\downarrow = 0.1n_\uparrow$, where $n_\uparrow$ and $n_\downarrow$ are the electron densities with up and down spins, respectively. Note that Mauger ascribed the unusual magnetization curve to the means of electron occupation in the spin-splitting band.[18]

IV. RESULTS AND DISCUSSION FOR GD-DOPED EUO

In the present section, we consider the effects of the on-site attractive potential E_C at Gd sites by applying the dynamical CPA to the model Hamiltonian for $Eu_{1-x}Gd_xO$ [i.e., Eq. (5)]. We treat the Gd concentration x and the electron density n independently.

A. Nature and properties of magnetic impurity states and/or impurity band tail

In Figs. 7 and 8, we show the lower-energy part of the DOS of $Eu_{1-x}Gd_xO$ with a lower Gd concentration of $x \lesssim 1.0\%$ in the PM and FM states, respectively. In the PM state, when $x \to 0$, a donor level appears at the energy level $\omega_P = -1.0314\Delta$, as shown by dot P in Fig. 7. The activation energy is estimated as $\omega_b - \omega_P = 0.0083\Delta = 0.029$ eV. Therefore the present model is consistent with the shallow-donor picture with an activation energy of 0.017 eV.[1] With increasing x, an

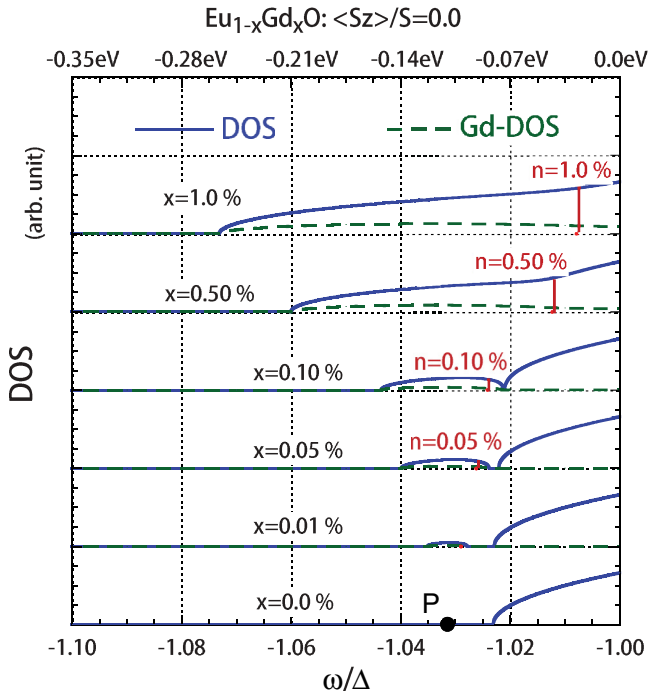

FIG. 7. (Color online) Lower-energy part of the DOS at paramagnetic temperatures $D(\omega)[=D_\uparrow(\omega)=D_\downarrow(\omega)]$ shown for $Eu_{1-x}Gd_xO$ with $x = 0.0$, 0.01, 0.05, 0.10, 0.50, and 1.0 %. The vertical lines indicate the Fermi levels ε_F for $n = x$. Dot P indicates the impurity level for $x \to 0$. The Gd-component DOS $xD^{Gd}(\omega)$ is shown by dashed lines. Along the upper abscissa, the $\omega + \Delta$ values with $\Delta = 3.5$ eV are shown in electron volts; note that the energy of the bottom of the model band ($\omega_0 = -\Delta$) is assigned to 0 eV.

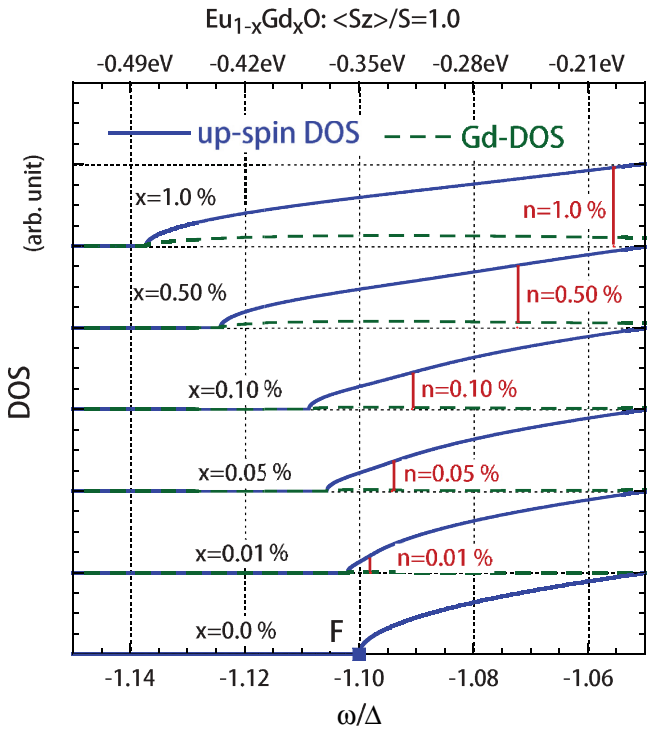

FIG. 8. (Color online) Lower part of the up-spin DOS at the ferromagnetic state $D_\uparrow(\omega)$ shown for $Eu_{1-x}Gd_xO$ with $x = 0.0$, 0.01, 0.05, 0.10, 0.50, and 1.0 %. The down-spin DOS $D_\downarrow(\omega)$ is not shown because it is negligible in the energy range used. The vertical lines indicate the Fermi levels ε_F for $n = x$. Dot F indicates the impurity level for $x \to 0$. The Gd-component DOS $xD^{Gd}_\uparrow(\omega)$ is shown by dashed lines.

impurity band forms at approximately the donor level; the total number of states of the impurity band is not $2x$ but $2x(S+1)/(2S+1) = 1.125x$ (see discussion below). When $x \gtrsim 0.10\%$, the impurity band merges into the host band, forming an impurity band tail; the band tail stretches to the low-energy side with a further increase in x. In Fig. 8, we show only the up-spin DOS because the down-spin DOS is negligible at energies in the FM state. Note that, for the present parameters, the energy of the donor level is estimated by Eq. (C7) as $\omega_F = -1.1\Delta$, which is in agreement with the bottom of the conduction band of EuO in the FM state (i.e., $-\Delta - IS$, see also Fig. 1); thus no impurity band forms separately. With increasing x, the band tail stretches to the low-energy side.

In Fig. 9, we show how the change in $\langle S_z\rangle/S$ accompanies the change in the spin-polarized DOS of $Eu_{1-x}Gd_xO$ with $x = 0.05\%$ as an example. In the PM state, an impurity band separated from the host band forms. With the development of magnetization, the impurity band soon merges into the host band to form the band tail; the band tail stretches to the low-energy side. Thus the impurity band and/or the band tail of $Eu_{1-x}Gd_xO$ is strongly affected by magnetization. The result shows that the shift in the Fermi level ε_F is approximately proportional to $\langle S_z\rangle$. The controversy of whether or not a minimum n or x is needed to increase T_C is closely related to such a low-x region of $Eu_{1-x}Gd_xO$.

To elucidate the nature of the magnetic impurity band and its effect on magnetism, here we investigate the case of deep impurity levels using $E_C = 0.8\Delta$; the other parameters are the same as those for $Eu_{1-x}Gd_xO$. In Fig. 10, the result for a spin-polarized DOS with $x = 0.10\%$ is shown. In the PM state, two impurity bands appear at approximately the impurity levels indicated by dots P and A: $\omega_P = -1.1821\Delta$ and $\omega_A = -1.0542\Delta$. The parallel (antiparallel) spin-coupling impurity band around dot P (A) is composed of electron states in which an electron spin strongly couples parallel (antiparallel) to the f spin; hereafter, we refer to the impurity bands as the P and A subbands. The number of states of the P subband is $2x(S+1)/(2S+1) = 1.125x$ and that of the A subband is $2xS/(2S+1) = 0.875x$; thus the total number of impurity states is $2x$. With the development of magnetization, the A subband shifts to the high-energy side and merges with the host band. On the other hand, the P subband shifts to the low-energy side by an amount proportional to $\langle S_z\rangle$, causing it to separate from the host band. In the FM state, the P subband is in agreement with the impurity band at approximately the impurity level F; $\omega_F = -1.2125\Delta$. The impurity band is composed of up-spin and down-spin states in the FM state; the number of up-spin states is x and that of down-spin states is $x/(2S+1) = 0.125x$. If some electrons are injected into the band, the electrons preferentially occupy the P subband. Note that the double occupation of electrons at the same site is substantially prevented because the P subband is only composed of electron states whose spin is coupled parallel to the f spin at the impurity site. Then, if $n \lesssim 1.125x$,

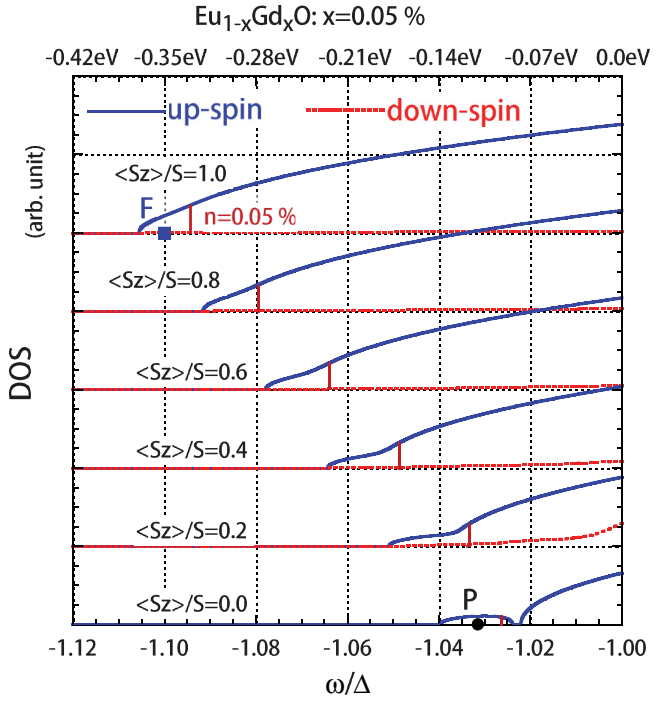

FIG. 9. (Color online) Lower part of the spin-polarized DOS of $Eu_{1-x}Gd_xO$ with $x = 0.05\%$ $D_\uparrow(\omega)$ and $D_\downarrow(\omega)$ shown for various $\langle S_z\rangle/S$ values. The vertical lines indicate the Fermi levels ε_F for $n = x = 0.05\%$. Dots P and F represent the impurity levels in the paramagnetic and ferromagnetic states, respectively.

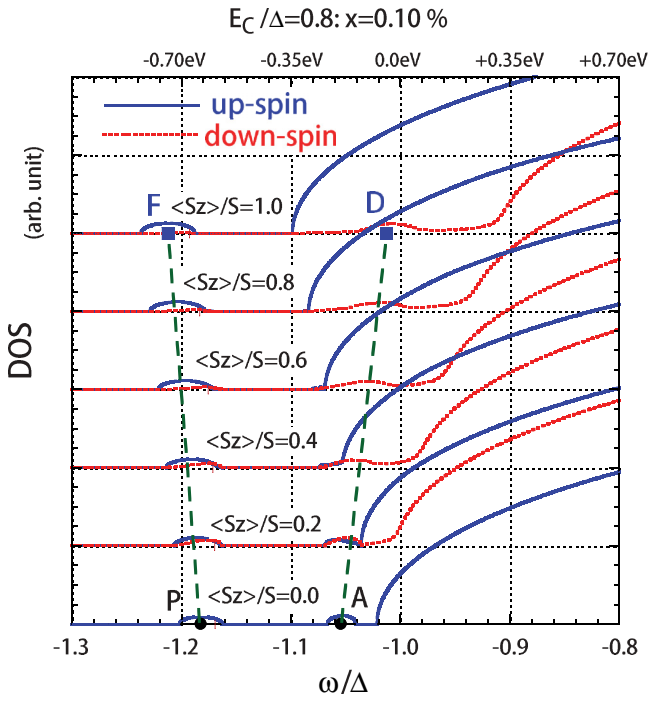

FIG. 10. (Color online) Result obtained by using $E_C/\Delta = 0.8$; the other parameters are the same as those of $Eu_{1-x}Gd_xO$. The lower part of the spin-polarized DOS $D_\uparrow(\omega)$ and $D_\downarrow(\omega)$ calculated with $x = 0.10\%$ is shown for various $\langle S_z\rangle/S$ values. Dots P and A indicate the impurity levels in the paramagnetic state and dots F and D indicate the impurity levels in the ferromagnetic state (see text). The dashed straight lines between P and F and between A and D are visual guides.

the total energy is estimated as

$$E(\langle S_z\rangle) \cong n\omega_P - \frac{\langle S_z\rangle}{S} n(\omega_P - \omega_F)\,. \tag{27}$$

Thus the effective field due to electrons in the impurity band is calculated as

$$h_2 = -\frac{d}{d\langle S_z\rangle} E(\langle S_z\rangle) \cong \frac{n}{S}(\omega_P - \omega_F) = \frac{n}{S}\,\frac{\Delta^2 IS}{4E_C[E_C + I(2S+1)]}\,. \tag{28}$$

The meaning of h_2 in Eq. (28) is clear. Electrons in the impurity band induce an effective field h_2 on f spins through the exchange interaction; h_2 is independent of $\langle S_z\rangle/S$.

Sutarto *et al.* reported that no threshold behavior is observed at Gd concentrations as low as $x \approx 0.2\%$.[13] Later, Mairoser *et al.* referred to a minimum electron density needed to induce a measurable increase in T_C; the minimum density is approximately $1 \times 10^{19}\text{cm}^{-3} = 0.034\%$, which corresponds to $x = 0.25$–1.0%.[17] The present result is compatible with the experimental results in both reports. There is a threshold Gd concentration x_c; $x_c \lesssim 0.1\%$. $x_c \approx 0.1\%$ is about one order of magnitude smaller than the values of 1.2–1.5% reported previously.[3,4,7] When $x \lesssim x_c$ at PM temperatures, an impurity band forms separately from the host band, so that each electron is weakly bound to a different Gd site; the electron spin strongly couples parallel to the f spin at the Gd site. The semilocalized electron induces a local effective field through the exchange interaction to polarize the f spins at the surrounding Eu sites. This is the so-called magnetic impurity state or trapped magnetic polaron.[37] The existence of the magnetic impurity state causes confusion in the measurement of T_C in such lightly Gd-doped EuO.

Here, we should emphasize that the magnetic impurity band in EuO is very different from that in diluted magnetic semiconductors (DMSs) such as $Gd_{1-x}Mn_xAs$.[38,39] In the case of a magnetic impurity band in DMSs, the hopping of carriers among magnetic sites causes ferromagnetism through a double-exchange (DE)-like mechanism. The mechanism of increasing T_C in Gd-doped EuO, however, is not the DE-like mechanism; the increase in T_C is due to conduction electrons in a broad band. The present picture of magnetic impurity states is also very different from the splitting donor level picture in an FM semiconductor proposed by Haas.[40]

B. Electronic and magnetic properties of Gd-doped EuO

In Figs. 11–13, we show the present results for $Eu_{1-x}Gd_xO$ with $x = 1.0, 7.0$, and 15%. When $x = 1.0\%$, as shown in Fig. 11(a), the band tail clearly exhibits the character of a magnetic band tail. $Q(\omega)$ at the Eu site shown in Fig. 11(b) is similar to that of EuO shown in Fig. 1(b). In contrast, $Q(\omega)$ at the Gd site shown in Fig. 11(c) is somewhat different. In the PM state, $Q(\omega)$ at the Gd site is very high at energies ω of approximately ω_P, but decreases rapidly at energies above ω_A. In the FM state, $Q(\omega) \approx 1.0$ at energies roughly over

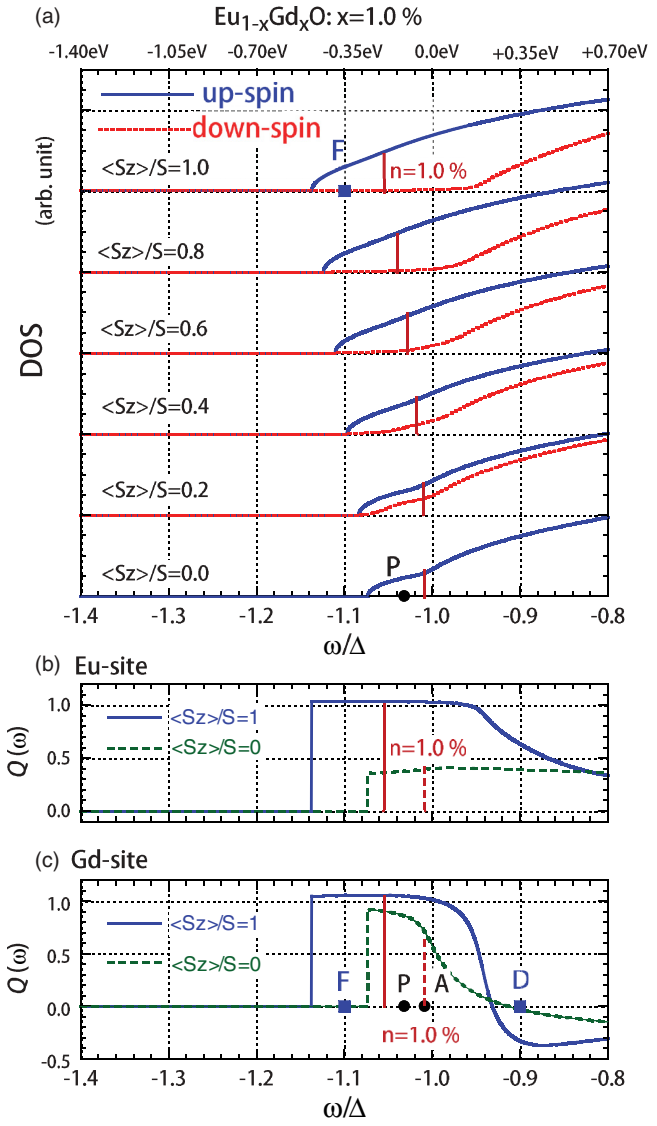

FIG. 11. (Color online) Results for $Eu_{1-x}Gd_xO$ with $x = 1.0\%$. In (a), the lower part of the spin-polarized DOS is shown for various $\langle S_z\rangle/S$ values; the solid line is for $D_\uparrow(\omega)$ and the dotted line is for $D_\downarrow(\omega)$. Each vertical line indicates the Fermi level ε_F for $n = x = 1.0\%$. In (b) and (c), the spin-coupling strength $Q(\omega)$ at the Eu site and Gd site are shown, respectively; the solid line is for $\langle S_z\rangle/S = 1$ and the dashed line is for $\langle S_z\rangle/S = 0$. Dots P, F, A, and D indicate the impurity levels ω_P, ω_F, ω_A, and ω_D, respectively (see text). The Fermi level ε_F is indicated by vertical lines; the dashed line is for $\langle S_z\rangle/S = 0.0$ and the solid line is for $\langle S_z\rangle/S = 1.0$.

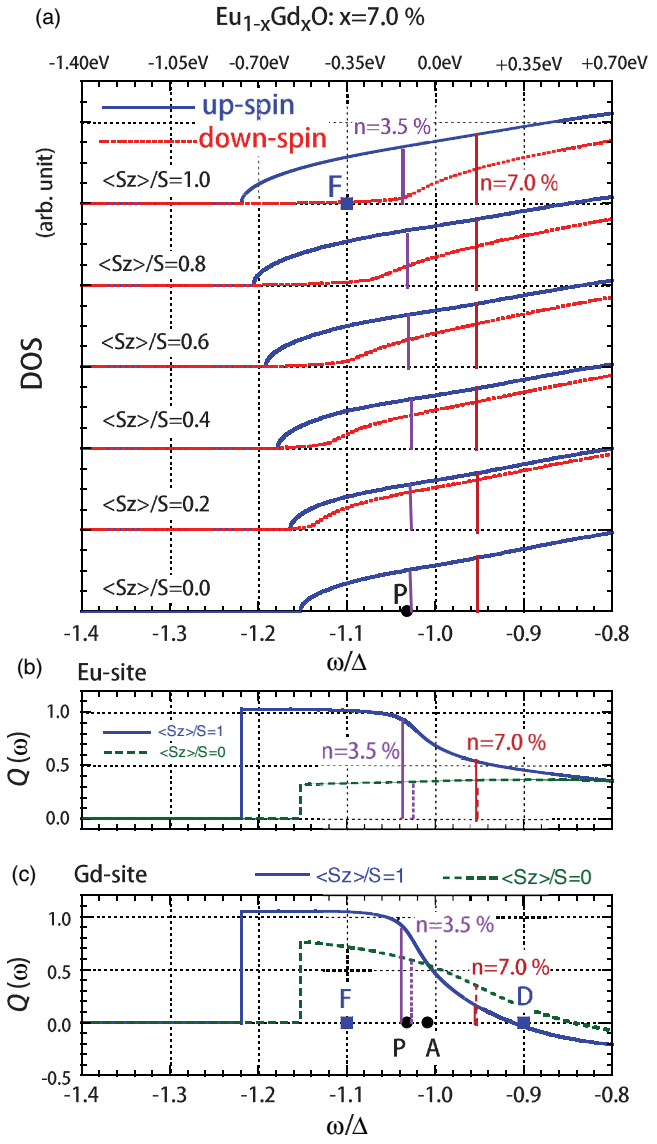

FIG. 12. (Color online) Same as Fig. 11, but for $x = 7.0\%$; the vertical lines indicate the Fermi level ε_F for $n = x = 7.0\%$ and $n = 0.5x = 3.5\%$.

the energy width $2IS$ from the bottom of the band; then $Q(\omega)$ decreases rapidly, even becoming negative at energies of approximately ω_D. Note again that P and F are the parallel spin-coupling impurity levels so that $Q(\omega) \approx 1.0$ therein; A and D are the antiparallel spin-coupling impurity levels so that $Q(\omega) \approx -1.0$ therein. At first glance, the DOSs shown in Figs. 12(a) and 13(a) are similar to that shown in Fig. 1(a), except that the band tail shifts to the low-energy side as a whole. It should be emphasized that the behavior of $Q(\omega)$ is also similar to that shown in Fig. 1(b); the energy width of high $Q(\omega)$ does not substantially change. In Figs. 12 and 13, we include the Fermi levels not only for $n = x$ but also for $n = 0.5x$.

In Figs. 14 and 15, we show the present results for $Eu_{1-x}Gd_xO$ calculated assuming that the electron density is equal to the Gd concentration (i.e., $n = x$). Comparing Fig. 14(a) with Fig. 2(a), the Fermi levels ε_F of $Eu_{1-x}Gd_xO$ are much lower than that of electron-doped EuO. Comparing Fig. 14(b) with Fig. 2(b), however, the energy shifts $\varepsilon_F(\langle S_z\rangle/S) - \varepsilon(0)$ are very similar to each other. Thus the n dependence of the T_C of $Eu_{1-x}Gd_xO$ with $n = x$ is similar to that of electron-doped EuO with the same n, although the T_C of $Eu_{1-x}Gd_xO$ is lower than that of electron-doped EuO, as is shown in Fig. 3. Comparing Fig. 15 with Fig. 4, both magnetization curves are similar to each other, although the feature of the unusual magnetization is so unclear that the flexure points are difficult to recognize in Fig. 15. The reason for the difference can be understood as follows. The attractive

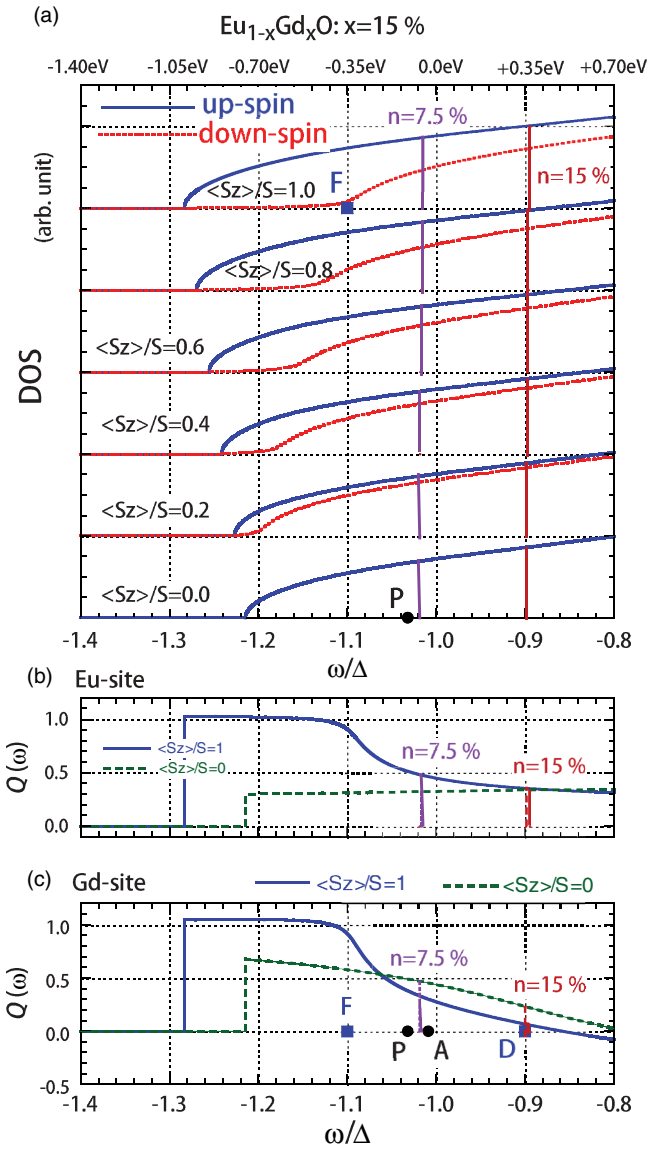

FIG. 13. (Color online) Same as Fig. 11, but for $x = 15\%$; the vertical lines indicate the Fermi level ε_F for $n = x = 15\%$ and $n = 0.5x = 7.5\%$.

potential E_C increases the number of electron states around the donor level in the band tail irrespective of the magnetic state. Thus E_C operates so that the difference in the bands between the PM and FM states becomes smaller, resulting in a smaller increase in T_C, and hiding the noticeable feature of the anomalous magnetization.

As an example of the electron density n not being in agreement with the Gd concentration x, we also investigated the case of $Eu_{1-x}Gd_xO$ with $n = 0.5x$. The result showed the high similarity of $Eu_{1-x}Gd_xO$ between $n = x$ and $0.5x$ (see T_C included in Fig. 3). The reason for the similarity is that the shapes of the spin-polarized DOSs calculated with different values of x are very similar, although the band shifts to the low-energy side depending on x. As a consequence, the electron density n precedes the Gd concentration x for the determination of the magnetization of $Eu_{1-x}Gd_xO$.

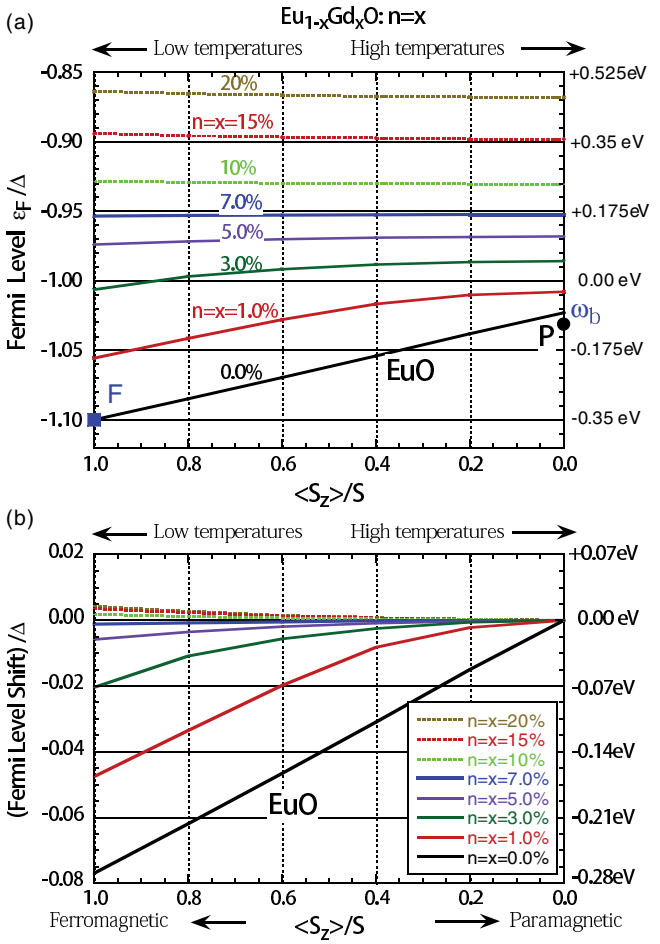

FIG. 14. (Color online) Same as Fig. 2, but for $Eu_{1-x}Gd_xO$ assuming $n = x$. Note that the scale in (a) is very different from that in Fig. 2.

C. Relationship between the Fermi level and the optical absorption edge

Here, we try to relate the present results for ε_F with the experimental observation of the optical absorption edge of undoped EuO and Gd-doped EuO on the assumption that the absorption edge corresponds to the electron transition from the $4f$ state to the Fermi level ε_F. In this work, we have calculated the $\langle S_z \rangle$ dependence of ε_F in three cases: electron-doped EuO (see Fig. 2), $Eu_{1-x}Gd_xO$ with $n = x$ (see Fig. 14), and $Eu_{1-x}Gd_xO$ with $n = 0.5x$. Comparing these three cases, the results for the energy shift of the Fermi level $\varepsilon_F(\langle S_z \rangle/S) - \varepsilon_F(0)$ are very similar. When $x = n = 0$, the present result is in agreement with that of EuO, suggesting that the bottom of the band shifts as $\varepsilon_F(\langle S_z \rangle/S) - \varepsilon_F(0) = -I_{\text{eff}}\langle S_z \rangle$;[22] $I_{\text{eff}}S = \omega_b + \Delta + IS = 0.0769\Delta = 0.27$ eV corresponds to the total redshift of EuO. As shown in Fig. 2(b), the total redshift decreases with increasing n and takes values of 0.188, 0.100, and 0.034 eV for $n = 1.0$,3.0, and 5.0%, respectively; for $n \gtrsim 10\%$, the present results even show a blue shift. As has already been discussed, the behavior of $\varepsilon_F(\langle S_z \rangle/S) - \varepsilon_F(0)$ is closely related to the n dependence of T_C. For the total redshifts of the absorption edge in Gd-doped EuO, the following values are obtained experimentally: 0.188 and 0.124 eV for $n = 0.54$

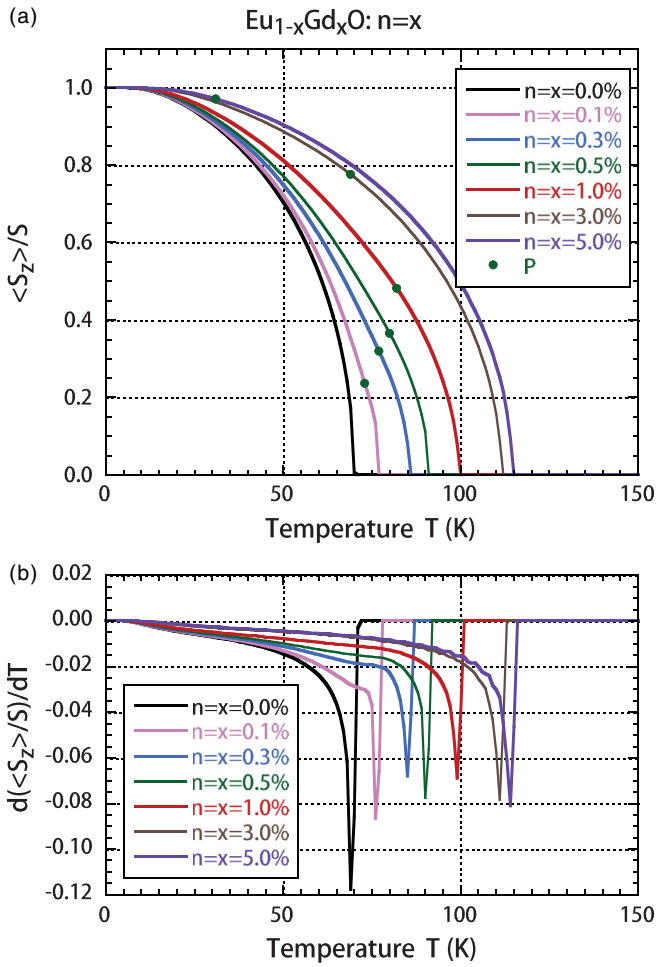

FIG. 15. (Color online) Same as Fig. 4, but for $Eu_{1-x}Gd_xO$ assuming $n = x$.

and 2.04 %,[1,5] and 0.20 and 0.12 eV for $Eu_{1-x}Gd_xO$ with $x = 1$ and 5%, respectively.[10] Therefore the present results well explain the n and/or x dependence of the total redshifts experimentally observed.

On the other hand, the present results for ε_F greatly differ among the three cases. In addition, the results experimentally reported are contradictory. According to Schoenes and Wachter,[5] the absorption edge of Gd-doped EuO in the PM state appears at a lower energy than that of EuO. However, according to Matsumoto *et al.*,[10] it appears at a higher energy than that of EuO. Therefore we cannot compare the present results with the experimental ones. A systematic study of the optical properties of high-quality samples of Gd-doped EuO is strongly desired.

V. CONCLUDING REMARKS

In the present study, we have calculated spin-polarized DOSs by applying the dynamical CPA to two models; we employ the s-f model Hamiltonian (3) for electron-doped EuO and the model Hamiltonian (5) for $Eu_{1-x}Gd_xO$. On the basis of the spin-polarized DOSs, we estimated the total energy of electrons interacting with f spins through an exchange interaction to obtain the free energy as a function of $\langle S_z\rangle/S$. Then, we obtain the magnetization $\langle S_z\rangle/S$ as a function of the temperature T by minimizing the free energy. On the basis of the present results, we try to answer the six questions presented in Introduction.

(i) There is an intrinsic limit to the electron-induced increase in T_C. With increasing n, T_C first increases rapidly up to $n \simeq n_1$, then progressively saturates, giving rise to a maximum at approximately n_M, and decreases gradually. The result for the spin-coupling strength $Q(\omega)$ shows that n_1 corresponds roughly to the electron density at which the Fermi energy ε_F reaches an energy $2IS$ higher than the bottom of the band in the FM state. When $n \lesssim n_1$, the energy gain of the exchange interaction is so fully obtained that the increase in n is accompanied by a rapid increase in T_C. For the electron-doped EuO, $n_1 \approx 5\%$. n_M is somewhat larger than n_1 and estimated as $n_M \approx 7\%$.

(ii) The anomalous magnetization curve occurs in a situation that the down-spin band is hardly occupied by doped electrons in the FM state.[20] The situation occurs when $n \lesssim 5\%$. If $\langle S_z\rangle$ is smaller than a certain value, both the up- and down-spin bands are populated, and then the magnetization curve becomes a standard curve. If $\langle S_z\rangle$ is larger than a certain value, however, few electrons occupy the down-spin states [see Fig. 1(a)]; then the electrons in the up-spin band act as an external field on the f spins. Therefore the magnetization curve is composed of two partial curves above and below a certain $\langle S_z\rangle$. This yields an anomalous magnetization. On the other hand, the present models do not explain the departure from the standard curve reported for $x \gtrsim 10\%$.[13]

(iii) There is a threshold of the Gd concentration x_c for increasing T_C: $x_c \lesssim 0.1\%$. When $x \lesssim x_c$ at PM temperatures, an electron weakly bound to Gd site forms the so-called magnetic impurity state or trapped magnetic polaron. The existence of the magnetic impurity state causes confusion in the measurement of T_C in the low-x region.

(iv) The attractive potential E_C at the donor Gd site makes the anomalous magnetization less clear and suppresses the increase in T_C. This is because the attractive potential E_C increases the electron states around the energy of the donor level in the band tail irrespective of the magnetic state. Thus E_C reduces the difference in the bands between the PM and FM states. However, an anomalous magnetization is experimentally observed in Gd-doped EuO with $0.1\% \lesssim x \lesssim 5\%$. One of the conventional explanations for the weakening of the attractive potential is the screening effect. When the impurity band merges into the host band ($x \gtrsim 0.1\%$), an electron cloud gathers around the Gd donor center so as to weaken the attractive Coulomb interaction; thus E_C becomes less effective.

(v) The electron density n mainly determines the magnetic properties of Gd-doped EuO. Comparing the two cases of $Eu_{1-x}Gd_xO$ with $n = x$ and $0.5x$, their results are very similar for the same n. However, we have to add that the present result does not clarify the cause of the low dopant activity reported by Mairoser *et al.*[17]

(vi) A large redshift of the optical absorption edge is closely related to the rapid increase in T_C with increasing n. The redshift corresponds to the gain of total electron energy, because the optical absorption is assigned to the electron transition from the $4f$ state to the Fermi level ε_F. Therefore

the decrease in total redshift with increasing n observed in Gd-doped EuO is consistently explained by the gradual increase in T_C as n approaches $n_1 \approx 5\%$. The present result even predicts a blue-shift of the optical absorption edge for $n \gtrsim 10\%$, although no optical experiment has reported this yet for such heavily doped EuO.

The present theory gives a consistent explanation for some of the electronic and magnetic properties of Gd-doped EuO. There are, however, some remaining issues for future study, even in the framework of the present model. For example, $\langle S_z \rangle$ for the f spin at the Gd site may be different from that at the Eu site, because electrons stay longer at the Gd site owing to the attractive potential E_C. The difference in $\langle S_z \rangle$ among the different sites results in different effective fields h. Treating the effect self-consistently assists the semilocalization of electrons such as magnetic polarons.[41] Furthermore, the nondegenerate effect of electrons becomes important, particularly in lightly doped EuO, although we assumed the electrons are degenerate throughout the present work. Another issue is the effect of the short-range order of f spins on electron states; with decreasing temperature, the optical absorption edge does not decrease as $-I_{\rm eff}\langle S_z \rangle$, but decreases in proportion to the spin correlation function.[5] Because the CPA is a single-site approximation, incorporating the spin correlation effect into the present frame is very difficult.[42]

Recently, many first-principles calculations have been performed.[43–48] Ingle and Elfimov[43] and Altendorf *et al.*[44] have calculated T_C as a function of n to show a maximum in T_C. However, they have not calculated the PM band structure for randomly oriented f spins; instead, they calculated it for antiferromagnetic (AFM) spin configurations. They theoretically evaluated T_C by comparing the energies of FM and AFM configurations. Thus, in their approach, the multiple-scattering effect is taken into account to a certain extent, whereas the effect of thermal fluctuation of f spins on the electron states is not considered. It has already been shown that the energy of the bottom of the AFM conduction band has a similar IS/Δ dependence to that calculated by the CPA for the PM state (see Fig. 7 in Ref. 49). In their calculations, therefore, the energy gain is considerably suppressed compared with the energy gain obtained using the VCA, resulting in a maximum in T_C. Wan *et al.* have used the dynamical-mean-field-theory (DMFT) to treat the thermal fluctuation.[45] It has been verified that T_C obtained by DMFT is very similar to that obtained by the dynamical CPA in the case of carrier-induced ferromagnetism in diluted magnetic semiconductors (see Fig. 3 in Ref. 50).

ACKNOWLEDGMENT

The author sincerely thanks Professor Naoki Honda for his kind advice and continuous encouragement.

APPENDIX A: EXPLICIT EXPRESSIONS FOR $G^{\rm Gd}_{\mu\nu}$

Here, for simplicity, the site-diagonal matrix elements of $G^{\rm Gd}$ in the Wannier representation, $\langle n\mu|G^{\rm Gd}|n\nu\rangle$, are written as $G^{\rm Gd}_{\mu\nu}$. To obtain the explicit expressions for $G^{\rm Gd}_{\mu\nu}$, we rewrite Eq. (9) as

$$G^{\rm Gd}\left(\omega - u^{\rm Gd}_n - \sum_\mu J_\mu a^\dagger_{n\mu} a_{n\mu}\right) = 1\,. \tag{A1}$$

Equation (A1) is written in the spin-matrix-element expression as

$$G^{\rm Gd}_{\uparrow\uparrow}(\omega + E_C + IS_z - J_\uparrow) + G^{\rm Gd}_{\uparrow\downarrow}(IS_+) = 1\,, \tag{A2a}$$

$$G^{\rm Gd}_{\uparrow\uparrow}(IS_-) + G^{\rm Gd}_{\uparrow\downarrow}(\omega + E_C - IS_z - J_\downarrow) = 0\,. \tag{A2b}$$

Here, S_z is the z component of the f spin: $S_+ = S_x + iS_y$ and $S_- = S_x - iS_y$. Equation (A2) comprises simultaneous equations containing $G^{\rm Gd}_{\uparrow\uparrow}$ and $G^{\rm Gd}_{\uparrow\downarrow}$, which can be solved after a somewhat complicated calculation using the commutation relationships between the components of **S** (but with no further approximations). The resulting expressions are

$$G^{\rm Gd}_{\uparrow\uparrow} = \frac{\omega + E_C - I(S_z+1) - J_\downarrow}{[\omega + E_C + IS_z - J_\uparrow][\omega + E_C - I(S_z+1) - J_\downarrow] - I^2\left[S(S+1) - S_z^2 - S_z\right]}\,, \tag{A3a}$$

$$G^{\rm Gd}_{\downarrow\downarrow} = \frac{\omega + E_C + I(S_z-1) - J_\uparrow}{[\omega + E_C - IS_z - J_\downarrow][\omega + E_C + I(S_z-1) - J_\uparrow] - I^2\left[S(S+1) - S_z^2 + S_z\right]}\,, \tag{A3b}$$

$$G^{\rm Gd}_{\uparrow\downarrow} = \frac{1}{[\omega + E_C + IS_z - J_\uparrow][\omega + E_C - I(S_z+1) - J_\downarrow] - I^2\left[S(S+1) - S_z^2 - S_z\right]}(-IS_-)\,, \tag{A3c}$$

$$G^{\rm Gd}_{\downarrow\uparrow} = \frac{1}{[\omega + E_C - IS_z - J_\downarrow][\omega + E_C + I(S_z-1) - J_\uparrow] - I^2\left[S(S+1) - S_z^2 + S_z\right]}(-IS_+)\,. \tag{A3d}$$

Note that the spin-diagonal matrix elements are written as $G^{\rm Gd}_{\uparrow\uparrow}(S_z)$ and $G^{\rm Gd}_{\downarrow\downarrow}(S_z)$ because they include S_z only. The expressions for $G^{\rm Eu}_{\mu\nu}$ are obtained after simply setting $E_C = 0$ in Eq. (A3).

APPENDIX B: SPIN-COUPLING STRENGTH $Q(\omega)$

Here, we show the calculation for the spin-coupling strength $Q(\omega)$ defined by Eq. (18):[51]

$$Q(\omega)|_{\rm Gd-site} = \left.\frac{\langle \delta(\omega - H)\boldsymbol{\sigma}\cdot\boldsymbol{S}\rangle/S}{\langle\delta(\omega - H)\rangle}\right|_{\rm Gd-site}\,. \tag{B1}$$

The denominator of Eq. (B1) is simply calculated as

$$\langle\delta(\omega - H)\rangle|_{\mathrm{Gd-site}} = D^{\mathrm{Gd}}_{\uparrow}(\omega) + D^{\mathrm{Gd}}_{\downarrow}(\omega)\,, \tag{B2}$$

where $D^{\mathrm{Gd}}_{\mu}(\omega)$ is the the local DOS with a μ spin at the Gd site. The numerator of Eq. (B1) is expanded as

$$\sum_{\mu\nu}\left\langle\delta(\omega - H)\boldsymbol{\sigma}_{\mu\nu}\cdot\frac{\boldsymbol{S}}{S}\right\rangle\Big|_{\mathrm{Gd-site}} = -\frac{1}{\pi S}\mathrm{Im}\langle[G^{\mathrm{Gd}}_{\uparrow\uparrow}(\omega) - G^{\mathrm{Gd}}_{\downarrow\downarrow}(\omega)]S_z + G^{\mathrm{Gd}}_{\uparrow\downarrow}(\omega)S_+ + G^{\mathrm{Gd}}_{\downarrow\uparrow}(\omega)S_-\rangle\,. \tag{B3}$$

For the PM state ($\langle S_z\rangle = 0$), Eq. (B3) is simply expressed as

$$\sum_{\mu\nu}\left\langle\delta(\omega - H)\boldsymbol{\sigma}_{\mu\nu}\cdot\frac{\boldsymbol{S}}{S}\right\rangle\Big|_{\mathrm{Gd-site}} = \frac{2}{\pi}\mathrm{Im}\frac{I(S+1)}{[\omega - J + E_C - I(S+1)][\omega - J + E_C + IS]}\,, \tag{B4}$$

where $J = J_{\uparrow} = J\downarrow$. For the FM state ($\langle S_z\rangle = S$), Eq. (B3) is expressed as

$$\sum_{\mu\nu}\left\langle\delta(\omega - H)\boldsymbol{\sigma}_{\mu\nu}\cdot\frac{\boldsymbol{S}}{S}\right\rangle\Big|_{\mathrm{Gd-site}} = -\frac{1}{\pi}\mathrm{Im}\frac{1}{\omega - J_{\uparrow} + E_C + IS} + \frac{1}{\pi}\mathrm{Im}\frac{\omega - J_{\uparrow} + E_C + I(S+1)}{[\omega - J_{\downarrow} + E_C - IS][\omega - J_{\uparrow} + E_C + I(S-1)] - 2I^2S}. \tag{B5}$$

Note that, in the classical spin limit (i.e., $1/S \to 0$), for the FM state,

$$Q(\omega)|_{\mathrm{Gd-site}} = \frac{D^{\mathrm{Gd}}_{\uparrow}(\omega) - D^{\mathrm{Gd}}_{\downarrow}(\omega)}{D^{\mathrm{Gd}}_{\uparrow}(\omega) + D^{\mathrm{Gd}}_{\downarrow}(\omega)}\,. \tag{B6}$$

In the classical spin limit, therefore, $Q(\omega)|_{\mathrm{Gd-site}} = 1$ at energies ω near the bottom of the band. In the present work, in contrast, $Q(\omega)|_{\mathrm{Gd-site}} \approx 1.04$ near the bottom of the band as a consequence of the quantum effect due to the finite spin value $S = 7/2$. The expressions for $Q(\omega)|_{\mathrm{Eu-site}}$ are obtained after simply setting $E_C = 0$ in the expressions above.

APPENDIX C: ENERGY OF IMPURITY LEVELS

For the PM state ($\langle S_z\rangle = 0$), the dynamical CPA condition Eq. (16) is written as

$$F(\omega) = (1-x)\left[\frac{p}{\omega + IS - J} + \frac{a}{\omega - I(S+1) - J}\right] + x\left[\frac{p}{\omega + E_C + IS - J} + \frac{a}{\omega + E_C - I(S+1) - J}\right], \tag{C1}$$

where $F = F_{\uparrow} = F_{\downarrow}$ and $J = J_{\uparrow} = J_{\downarrow}$; $p = (S+1)/(2S+1)$ and $a = S/(2S+1)$. When the Gd concentration tends to zero ($x \to 0$), Eq. (C1) reduces to the CPA condition for EuO:

$$F(\omega) = \frac{p}{\omega + IS - J} + \frac{a}{\omega - I(S+1) - J}\,. \tag{C2}$$

In the limit of $x \to 0$, the second term of Eq. (C1) can have a physical meaning only when the denominator is 0. This gives the condition for the energy of the impurity levels. At PM temperatures, two impurity levels appear at energies $\omega = \omega_{\mathrm{P}}$ and ω_{A}:

$$\omega_{\mathrm{P}} = -E_C - IS + J\,, \tag{C3a}$$

$$\omega_{\mathrm{A}} = -E_C + I(S+1) + J\,. \tag{C3b}$$

$\omega_{\mathrm{P}}(\omega_{\mathrm{A}})$ is the energy of an impurity electron whose spin is parallel (antiparallel)-coupled with the f spin at the Gd site. Substituting the $\omega = \omega_{\mathrm{P}}$ of Eq. (C3a) into Eq. (C2), we obtain $F(\omega_{\mathrm{P}})$. Next, using the relation $J = F\Delta^2/4$ [see Eq. (15)] in Eq. (C3a), we obtain the energy of a parallel spin-coupling impurity level as

$$\omega_{\mathrm{P}} = -E_C - IS - \frac{\Delta^2[E_C + I(S+1)]}{4E_C[E_C + I(2S+1)]}\,. \tag{C4}$$

The energy of an antiparallel spin-coupling impurity level is also obtained as

$$\omega_{\mathrm{A}} = -E_C + I(S+1) - \frac{\Delta^2(E_C - IS)}{4E_C[E_C - I(2S+1)]}. \tag{C5}$$

For the FM state ($\langle S_z\rangle = S$), the dynamical CPA condition Eq. (16a) is written as

$$F_{\uparrow}(\omega) = (1-x)\frac{1}{\omega + IS - J_{\uparrow}} + x\frac{1}{\omega + E_C + IS - J_{\uparrow}}. \tag{C6}$$

By a similar consideration to that above, we obtain the energy of an impurity electron with an up-spin at the Gd site as

$$\omega_{\mathrm{F}} = -E_C - IS - \frac{\Delta^2}{4E_C}\,. \tag{C7}$$

The energy of the impurity electron with a down spin, however, cannot be obtained. For $S_z = S$, Eq. (16b) is written as

$$F_\downarrow(\omega) = (1-x)\frac{\omega + I(S-1) - J_\uparrow}{[\omega - IS - J_\downarrow][\omega + I(S-1) - J_\uparrow] - 2I^2S} + x\frac{\omega + E_C + I(S-1) - J_\uparrow}{[\omega + E_C - IS - J_\downarrow][\omega + E_C + I(S-1) - J_\uparrow] - 2I^2S}. \tag{C8}$$

In Eq. (C8), $F_\downarrow(\omega)$ includes $J_\uparrow$, because the electron can flip its spin while the total spin ($=S-1/2$) is conserved at the Gd site. The spin-flip process is a quantum effect due to the finiteness of the f spin.[22] As we cannot obtain the energy for a finite spin S, we simply estimate the energy in the case of the classical spin limit [i,e., $1/S \to 0$, thus $I^2S = (IS)^2/S \to 0$]. The energy of an impurity electron with a down-spin for a classical spin S is simply obtained by changing $-IS$ to $+IS$ in Eq. (C7):

$$\omega_D = -E_C + IS - \frac{\Delta^2}{4E_C}. \tag{C9}$$

For the parameters of $Eu_{1-x}Gd_xO$ ($S = 7/2$, $\Delta = 3.5$ eV, $IS = 0.1\Delta = 0.35$ eV, $E_C = 0.5\Delta = 1.75$ eV), we obtain $\omega_P/\Delta = -1.0314$, $\omega_A/\Delta = -1.0083$, $\omega_F/\Delta = -1.1$, and $\omega_D/\Delta = -0.9$. For the parameters used in Fig. 10 ($E_C = 0.8\Delta = 2.8$ eV, the others are the same as those for $Eu_{1-x}Gd_xO$), $\omega_P/\Delta = -1.1821$, $\omega_A/\Delta = -1.0542$, $\omega_F/\Delta = -1.2125$, and $\omega_D/\Delta = -1.0125$.

*taka@gen.kanagawa-it.ac.jp

[1] P. Wachter, in *Handbook on Physics and Chemistry of Rare Earths*, edited by K. A. Gschneidner and L. Eyring (North-Holland, Amsterdam, 1979), p. 507.
[2] M. W. Shafer and T. R. McGuire, J. Appl. Phys. **39**, 588 (1968).
[3] A. A. Samokhvalov, B. A. Gizhevskii, M. I. Simonova, and N. I. Solin, Sov. Phys. Solid State **14**, 230 (1972).
[4] A. A. Samokhvalov, T. I. Arbuzova, M. I. Simonova, and L. D. Fal'kovskaya, Sov. Phys. Solid State **15**, 2459 (1974).
[5] J. Schoenes and P. Wachter, Phys. Rev. B **9**, 3097 (1974).
[6] A. Mauger, C. Godart, M. Escorne, J. Achard, and J. Desfours, J. Phys. **39**, 1125 (1978).
[7] A. Mauger, M. Escorne, C. Godart, J. Desfours, and J. Achard, J. Phys. Colloques **41**, C5 (1980).
[8] A. Mauger and C. Godart, Phys. Rep. **141**, 51 (1986).
[9] H. Rho, C. S. Snow, S. L. Cooper, Z. Fisk, A. Comment, and J. Ph. Ansermet, Phys. Rev. Lett. **88**, 127401 (2002).
[10] T. Matsumoto, K. Yamaguchi, M. Yuri, K. Kawaguchi, N. Koshizaki, and K. Yamada, J. Phys.: Condens. Matter **16**, 6017 (2004).
[11] A. Comment, J.-P. Ansermet, C. P. Slichter, H. Rho, C. S. Snow, and S. L. Cooper, Phys. Rev. B **72**, 014428 (2005).
[12] H. Ott, S. J. Heise, R. Sutarto, Z. Hu, C. F. Chang, H. H. Hsieh, H. J. Lin, C. T. Chen, and L. H. Tjeng, Phys. Rev. B **73**, 094407 (2006).
[13] R. Sutarto, S. G. Altendorf, B. Coloru, M. M. Sala, T. Haupricht, C. F. Chang, Z. Hu, C. Schusler-Langeheine, N. Hollmann, H. Kierspel *et al.*, Phys. Rev. B **80**, 085308 (2009).
[14] H. Miyazaki, H. J. Im, K. Terashima, S. Yagi, M. Kato, K. Soda, T. Ito, and S. Kimura, Appl. Phys. Lett. **96**, 232503 (2010).
[15] P. Liu, J. Tang, J. A. C. Santana, K. D. Belashchenko, and P. A. Dowben, J. Appl. Phys. **109**, 07C311 (2011).
[16] M. Barbagallo, N. D. M. Hine, J. F. K. Cooper, N.-J. Steinke, A. Ionescu, C. H. W. Barnes, C. J. Kinane, R. M. Dalgliesh, T. R. Charlton, and S. Langridge, Phys. Rev. B **81**, 235216 (2010).
[17] T. Mairoser, A. Schmehl, A. Melville, T. Heeg, L. Canella, P. Boni, W. Zander, J. Schubert, D. E. Shai, E. J. Monkman *et al.*, Phys. Rev. Lett. **105**, 257206 (2010).
[18] A. Mauger, Phys. Status Solidi B **84**, 761 (1977).
[19] M. Arnold and J. Kroha, Phys. Rev. Lett. **100**, 046404 (2008).
[20] M. Takahashi, J. Phys. Soc. Jpn. **80**, 075001 (2011).
[21] M. Takahashi, Materials **3**, 3740 (2010).
[22] M. Takahashi and K. Mitsui, Phys. Rev. B **54**, 11298 (1996).
[23] P. G. Steeneken, L. H. Tjeng, I. Elfimov, G. A. Sawatzky, G. Ghiringhelli, N. B. Brookes, and D.-J. Huang, Phys. Rev. Lett. **88**, 047201 (2002).
[24] S. J. Cho, Phys. Rev. B **1**, 4589 (1970).
[25] D. B. Ghosh, M. De, and S. K. De, Phys. Rev. B **70**, 115211 (2004).
[26] M. Stier and W. Nolting, Phys. Rev. B **78**, 144425 (2008).
[27] A. Sharma and W. Nolting, Phys. Rev. B **78**, 054402 (2008).
[28] P. Sinjukow and W. Nolting, Phys. Rev. B **69**, 214432 (2004).
[29] C. Santos and W. Nolting, Phys. Rev. B **65**, 144419 (2002).
[30] R. Schiller and W. Nolting, Phys. Rev. Lett. **86**, 3847 (2001).
[31] R. Metzke and W. Nolting, Phys. Rev. B **58**, 8579 (1998).
[32] W. Nolting, S. Rex, and S. M. Jaya, J. Phys.: Condens. Matter **9**, 1301 (1997).
[33] K. Kubo, J. Phys. Soc. Jpn. **36**, 32 (1974).
[34] H. Shiba, Prog. Theor. Phys. **46**, 77 (1971).
[35] A. Gonis, *Green Functions for Ordered and Disordered Systems*, Studies in Mathematical Physics 4 (North-Holland, Amsterdam, 1992).
[36] M. Takahashi, Phys. Rev. B **60**, 15858 (1999).
[37] M. Takahashi, Ph.D. thesis, Tohoku University, 1981.
[38] M. Takahashi and K. Kubo, Phys. Rev. B **66**, 153202 (2002).
[39] M. Takahashi and K. Kubo, J. Phys. Soc. Jpn. **72**, 2866 (2003).
[40] C. Haas, Phys. Rev. **168**, 531 (1968).
[41] M. Takahashi and T. Kasuya, J. Phys. Soc. Jpn. **52**, 3127 (1983).
[42] M. Takahashi, K. Mitsui, and M. Umehara, Phys. Rev. B **48**, 17053 (1993).
[43] N. J. C. Ingle and I. S. Elfimov, Phys. Rev. B **77**, 121202 (2008).
[44] S. G. Altendorf, N. Hollmann, R. Sutarto, C. Caspers, R. C. Wicks, Y.-Y. Chin, Z. Hu, H. Kierspel, I. S. Elfimov, H. H. Hsieh *et al.*, Phys. Rev. B **85**, 081201 (2012).

[45]X. Wan, J. Dong, and S. Y. Savrasov, Phys. Rev. B **83**, 205201 (2011).
[46]S. J. Blundell, T. Lancaster, F. L. Pratt, P. J. Baker, W. Hayes, J. P. Ansermet, and A. Comment, Phys. Rev. B **81**, 092407 (2010).
[47]J. M. An, S. V. Barabash, V. Ozolins, M. van Schilfgaarde, and K. D. Belashchenko, Phys. Rev. B **83**, 064105 (2011).
[48]J. A. ColonSantana, J. M. An, N. Wu, K. D. Belashchenko, X. Wang, P. Liu, J. Tang, Y. Losovyj, I. N. Yakovkin, and P. A. Dowben, Phys. Rev. B **85**, 014406 (2012).
[49]M. Takahashi, Phys. Rev. B **55**, 6950 (1997).
[50]M. Takahashi, N. Furukawa, and K. Kubo, J. Magn. Magn. Mater. **272–276**, 2021 (2004).
[51]M. Takahashi, Phys. Rev. B **70**, 035207 (2004).